

**Executive Summary of the Thesis**

**LOW COHERENCE INTERFEROMETRIC TECHNIQUES  
FOR IMAGING AND OPTICAL CHARACTERIZATION  
OF CELLS AND TISSUES**

A Thesis submitted to

**The Maharaja Sayajirao University of Baroda**

For The Award of Degree of

**DOCTOR OF PHILOSOPHY**

**IN**

**APPLIED PHYSICS**

By

**Mugdha Joglekar**

OPTICS LABORATORY  
DEPARTMENT OF APPLIED PHYSICS  
FACULTY OF TECHNOLOGY AND ENGINEERING  
THE MAHARAJA SAYAJIRAO UNIVERSITY OF BARODA  
VADODARA - 390001, GUJARAT, INDIA

**February 2022**

## Table of content

Table of content .....	i
List of figures .....	v
Abstract .....	1
Chapter 1 .....	3
Introduction.....	3
1.1 Methods to perform phase contrast imaging .....	5
1.2 Gabor Digital holographic Microscopy.....	5
1.3 Off-axis Digital Holographic Microscopy .....	7
1.4 Two beam off axis and common path geometries.....	8
1.5 Common Path Self-Refencing Digital Holographic Microscopy .....	10
1.6 Fringe Projection Technique .....	11
1.7 Large field of view self-referencing lens-less Holographic Microscopy .....	12
1.8 Low-cost Optical Coherence Tomographic System using LEDs.....	13
1.9 Summary of the Thesis.....	14
1.9.1 Chapter 1: Introduction.....	14
1.9.2 Chapter 2: Coherence .....	14
1.9.3 Chapter 3: Fringe Projection Technique.....	15
1.9.4 Chapter 4: Theory of holography .....	15
1.9.5 Chapter 5: Wide field of view common path self-referencing digital holographic microscopy employing LED.....	15
1.9.6 Chapter 6: Large field of view self-referencing lens-less Holographic Microscopy .....	16
1.9.7 Chapter 7: Low-cost Optical Coherence Tomographic System using LEDs .....	16
1.9.8 Chapter 8: Conclusion and future scope.....	16
Chapter 2 .....	17
Introduction to Coherence.....	17
2.1 Coherence.....	18
2.1.1 Temporal Coherence.....	18
2.1.2 Spatial Coherence .....	21
Chapter 3.....	27
Shape measurement of phase object and quantitative 3D imaging of dynamic micro-objects using fringe projection technique.....	27
3.1 Introduction .....	27
3.2 Transmission mode Fringe Projection Technique.....	29

3.3 Shape Measurement of Phase Objects using Fringe Projection Technique.....	31
3.3.1 Experimental Setup.....	31
3.4 Simulations.....	32
3.4.1 Simulation setup.....	33
3.4.2 Simulated objects.....	34
3.4.3 Image analysis.....	35
3.5 Experimental Results of Shape reconstruction of Phase Objects.....	37
3.6 Fringe projection microscope in transmission mode.....	41
3.7 Experimental results of shape measurement of micro-objects.....	42
3.8 Conclusion.....	46
Chapter 4.....	48
Theory of Digital holography.....	48
4.1 Recording of Holograms.....	48
4.2 Reconstruction of Holograms.....	49
4.3 Numerical propagation using Angular Spectrum approach.....	51
4.4 Retrieval of intensity and phase of object wavefront.....	54
4.5 Phase difference and object thickness.....	55
Chapter 5.....	58
Wide field of view off axis common path self-referencing digital holographic microscopy using low coherent source.....	58
5.1 Exploiting coherence properties of LEDs.....	58
5.2 Incorporating LED in common path self-referencing geometries.....	59
5.2.1 Resolution of the system.....	60
5.2.2 Calibration.....	60
5.2.3 Spatial stability.....	60
5.2.4 Temporal stability.....	60
5.2.5 Application in biomedical imaging.....	61
5.3 Self referencing digital holographic microscopy using Fresnel Biprism.....	61
5.3.1 Self-referencing digital holographic microscopy using He-Ne and a Fresnel Biprism..	63
5.3.1.1 Calibration.....	63

5.3.2.3 Calibration.....	68
5.3.2.4 Imaging Red blood cells.....	68
5.3.2.5 Improvement in lateral resolution .....	70
5.4 Self-referencing digital holographic interference microscopy using Lloyd’s mirror interferometer with increased field of view.....	71
5.4.1 Compact, low cost, large field-of-view Lloyds mirror digital holographic microscope using laser diode module .....	72
5.4.1.1 Temporal stability .....	75
5.4.1.2 Field of view improvement .....	75
5.4.1.3 Calibration.....	76
5.4.1.4 Imaging Red blood cells.....	77
5.4.2 Digital holographic microscopy using LED and Lloyd’s mirror.....	78
5.4.2.1 Calibration.....	79
5.4.2.2 Imaging Red blood cells.....	80
5.5 Digital holographic microscopy using Sagnac interferometer.....	81
5.5.1 Digital holographic microscopy using Sagnac interferometer and He-Ne laser.....	82
5.5.1.1 Calibration.....	83
5.5.1.2 Imaging Red blood cells.....	84
5.5.2 Sagnac Digital Holographic Microscopy exploiting the coherence properties of LED .84	
5.5.2.1 Temporal stability .....	85
5.5.2.2 Calibration.....	86
5.5.2.3 Imaging Red blood cells.....	87
5.6 Conclusion.....	88
Chapter 6.....	90
Lens-less Off-axis Self-Referencing Digital Holographic Microscopy.....	90
6.1 Introduction .....	90
6.2 Lens-less Common path Off-axis Digital Holographic Microscope.....	91
6.3 Theoretical background .....	91
6.3.1 Axial and Transverse Magnifications .....	94
6.4 Experimental Setup.....	95
6.5 Result and Discussion.....	96
6.5.1 Temporal stability .....	96
6.5.2 System Calibration and imaging capability: .....	97

6.6.1 Result and discussion.....	101
6.7 Conclusion.....	102
Chapter 7.....	104
Development of FD-OCT system employing LED and a Webcam .....	104
7.1 Introduction .....	104
7.2 Basic theory of Optical Coherence Tomography .....	106
7.3. Theoretical formulation .....	107
7.3.1 Time Domain OCT .....	109
7.3.2 Fourier Domain OCT.....	109
7.4 Experimental Setup.....	110
7.5 Result and discussion.....	113
7.5.1 Axial scanning of a mirror .....	113
7.5.2 Two mirrors at different depths .....	116
7.5.3 Sample with multiple structures.....	118
7.6 Conclusions .....	121
Chapter 8.....	122
Conclusion and future scope.....	122
References.....	125

## List of Figures

Fig 1. 1 Schematic of in-line digital holography configuration	7
Fig 1.2 Schematic of Mach-Zehnder interferometer configuration for digital holographic microscopy	8
Fig 1. 3 Schematic of Lateral shearing geometry	10
Fig 1. 4 Block diagram of Fringe projection technique	12
Fig 1. 5 Block diagram of Lens-less digital holographic technique	13
Fig 2. 1 Michelson interferometer	19
Fig 2. 2 Young's double slit interferometer	22
Fig 2. 3 Pictorial representation of temporal and spatial coherence in the case of plane waves	25
Fig 3.1 Recorded modulation of line pattern projected through a lens.	29
Fig 3.2 Propagation of light through axi-symmetric object	30
Fig 3.3 Transmission mode FPT for shape measurement of phase objects	32
Fig 3.4 (a) 3D schematic of the transmission mode fringe projection device. (b) Photograph of the table-top setup	32
Fig 3.5 (a) Projected line pattern imaged by digital array (b) Variation of intensity pattern along the line shown in fig 3.4 (a)	32
Fig 3.6 Optical system configuration for imaging the structured pattern projected through object under investigation. A magnification of 1 is used in the simulations	33
Fig 3.7 Phase of the simulated bi-prism. (a) Phase distribution in false color, where white grey value represents a normalized phase of 1 rad. (b) Normalized phase distribution along the red dotted line in Fig 3.7 (a). This phase is directly proportional to optical path length	34
Fig 3.8 Simulated line patterns at the detector array (image plane) for bi-prisms of different optical thicknesses (a) Optical thickness= $\lambda$ (b) Optical thickness= $5\lambda$ (c) Optical thickness= $7\lambda$ and (d) Optical thickness= $10\lambda$ , ( $\lambda=627\text{nm}$ ).	34
Fig 3.9 Flow chart of the object shape determination process	35
Fig 3.10 simulation results for biprism (a) Fourier spectrum of modulated structured pattern. (b) Filtered Fourier spectrum. (c) Gradient phase difference obtained by subtracting gradient phase due to carrier line pattern from gradient phase due to object line pattern. (d) Gradient phase along the y direction. (e) Phase profile obtained after numerical integration along y-	

direction. (f) Three- dimensional rendering of object shape profile in terms of obtained phase. 36

Fig 3.11 (a) Reconstructed phase profile (after numerical integration) for simulated objects as a function of object optical thickness (in terms of wavelength of source). (b) Maximum value of reconstructed phase as a function of object maximum optical thickness. 37

Fig 3. 12 Simulation results with right angular cone as object. (a) Simulated intensity pattern at the detector plane. (b) Reconstructed phase distribution. 37

Fig 3.13 Results of shape reconstruction with biprism as the object using a  $4.65\mu\text{m}$  pixel pitch CCD array as the recording device (a) Image of the line pattern recorded with the biprism placed in the field of view. (b) Image of the same line pattern recorded after removing the biprism (reference pattern). (c) Obtained gradient phase profile of the object after phase subtraction. (d) Line profile of the gradient phase. (e) Cross-sectional shape profile of the object after numerical integration of gradient phase. (f) Three-dimensional rendering of the shape of the bi-prism in terms of the recovered phase (obtained after numerical integration along each line along which there is variation in gradient phase). 38

Fig 3.14 Results of shape reconstruction for a cylindrical rod. Recording device was CCD camera (a) Image of the line pattern recorded with the rod placed in the field of view. (b) Image of the same line pattern recorded after removing the rod (reference pattern). (c) Obtained gradient phase profile of the object after phase subtraction. (d) Line profile of the gradient phase. (e) Cross-sectional shape profile of the object after numerical integration of gradient phase. (f) 3D rendering of the shape of the cylinder in terms of the recovered phase. 39

Fig 3.15 Results of shape reconstruction for a cylindrical lens as the object. Recording device was CCD camera. Only half the field of view is covered by the lens. (a) Image of the line pattern recorded with the lens placed in the field of view. (b) Image of the same line pattern recorded after removing the lens (reference pattern). (c) Obtained gradient phase profile of the object after phase subtraction. (d) Line profile of the gradient phase. (e) Cross-sectional shape profile of the object after numerical integration of gradient phase. (f) Three-dimensional rendering of the shape of the cylindrical lens in terms of the recovered phase. 39

Fig 3.16 Results of shape reconstruction for a bi-prism. Recording device was a smart-phone camera. (a) Image of the line pattern recorded with the bi-prism placed in the field of view. (b) Image of the same line pattern recorded after removing the bi-prism (reference pattern). (c) Three-dimensional rendering of the shape of the bi-prism lens in terms of the recovered phase. (d) Cross-sectional shape profile of the object 40

Fig 3.17 Results of shape reconstruction for a cylindrical rod. Recording device was a smart-phone camera. (a) Image of the line pattern recorded with the cylindrical lens placed in the field of view. (b) Image of the same line pattern recorded after removing the lens (reference pattern). (c) Three-dimensional rendering of the shape of the cylindrical lens in terms of the recovered phase. (d) Cross-sectional shape profile of the object. 40

Fig 3.18 Results of shape reconstruction for a cylindrical lens. Recording device was a smart-phone camera. (a) Image of the line pattern recorded with the cylindrical lens placed in the field of view. (b) Image of the same line pattern recorded after removing the lens (reference pattern). (c) Three-dimensional rendering of the shape of the cylindrical lens in terms of the recovered phase. (d) Cross-sectional shape profile of the object. 41

Fig 3.19 (a) Transmission mode quantitative 3D fringe projection microscope. (b) schematic representation of the line pattern. 42

Fig 3.20 (a) shows the 3D schematic of the developed system (b) shows the photograph of the developed system with different parts marked. The web cam was mounted near to the objective lens and so the magnification is around 15x. This was measured using microspheres of known size. 42

Fig 3. 21 Recorded line patterns (a) with and (b) without the object in the field of view. Spatial frequency spectrum (c) with object and (d) without object in the field of view. (e) Wrapped gradient phase obtained after phase subtraction. (f) Obtained gradient phase after phase unwrapping. (g) Phase obtained after numerical integration along horizontal direction. (h) Three-dimensional thickness distribution as a function of phase. 43

Fig 3. 22 (a) Recorded image for red blood cells. (b) Portion inside the rectangular box showing the modulation of the line pattern 44

Fig 3. 23 Quantitative imaging of human red blood cells. (a) unwrapped gradient phase profile. (b) Computed cell shape after numerical integration. Arrow in Fig 3.23 (a) shows direction of integration. The inset in Fig 3.23 (b) shows the cross-sectional profile of phase variation along the vertical line which indicated the donut profile of the cell. 44

Fig 3. 24 Temporal stability of the setup 45

Fig 3. 25 Phase profile of a healthy human red blood cell at different time instances. Time variation of the phase profiles at the points on the phase map at  $t=0s$  are computed and is shown in Fig 3.26 46

Fig 3.26 Time evolution of the phase profile at different spatial points along with their standard deviation (fluctuation). 46

Fig 4.2 Formation of hologram due to superposition of the object and the reference wavefronts at the detector plane. Carrier fringes are modulated in the region where the object exists. 48

Fig 4.3 Digital hologram reconstruction. Reference wave gets scattered from the structures of the hologram. It is numerically propagated to the position where the object existed (virtual image) 50

Fig 4.4 Position of the object (magnified image) and the hologram (detector) plane in DHIM. The object plane (magnified image plane) is situated either at the detector or very near to it. 51

Fig 4.5 Scattered wavefront as a collection of plane waves travelling in different directions (angle). The scattering angle is decided by the spatial frequency of the object (smaller objects, higher spatial frequencies) scatter at higher angles. An object with sinusoidal intensity variation (like a hologram), will give rise to only three scattered components (only one frequency component) 52

Fig 4.6 Numerical reconstruction of digital holograms using ASP approach. Reference wave illuminating the hologram generates the angular spectrum at the hologram plane ( $z=0$ ), which is filtered (to obtain angular spectrum of object wavefront at the hologram plane) and then propagated to the image plane using free space propagation function 52

Fig 4. 7 (a) Hologram illuminated by the reference wavefront. (b) Power spectrum of the hologram obtained after Fourier transform, where three components (un-diffracted reference, real object and virtual object) can be seen. (c) Filtered spectrum, which contains only the spatial frequencies corresponding to object alone. This is then propagated to the image plane 53

Fig 4.8 Object hologram of the  $15\mu\text{m}$  diameter polystyrene sphere immersed in oil. (b) Background hologram (microscope immersion oil) 55

Fig 4.9 Quantitative phase reconstruction from digital holograms. (a) Continuous phase difference obtained in the case of  $15\mu\text{m}$  diameter polystyrene microspheres. (b) Thickness distribution of the micro-sphere obtained by using the refractive index difference in Eq. (4.17). (c) Cross sectional thickness profile of the microsphere along the dashed line in Fig. 4.8a 56

Fig 5.1 Diameter of the spatial coherence area increases upon demagnifying the light emitting area of the source. 59

Fig 5.2 A typical Fresnel Biprism based interferometer 62

Fig 5.3 2D schematic of the common path self-referencing digital holographic microscope employing He-Ne laser and Fresnel Biprism interferometer 63

Fig 5.4 (a) recorded hologram of polystyrene beads (b) continuous phase distribution obtained after unwrapping (c) thickness distribution of the Polystyrene beads (d) cross-sectional thickness of the polystyrene microsphere. He-Ne laser source is used to illuminate the sample. 64

Fig 5.5 (a) recorded holograms of the RBCs (b) continuous phase distribution after unwrapping (c) thickness distribution of the RBCs (d) line profile of the thickness distribution. He-Ne laser source is used to illuminate the sample. 65

Fig 5.6 (a) shows the 3D schematic of the common path self-referencing digital holographic interference microscope employing a pair of Fresnel biprisms and LED source (b) Tabletop setup in the laboratory (VideoV1 shows the working of the tabletop setup) 66

Fig 5.7 Spatial stability (a) spatially varying optical path length using laser source (b) histogram of the spatial thickness variation along with the standard computed standard deviation value

for laser source. (c) spatially varying thickness using LED source (d) histogram of the spatial thickness along with the standard computed standard deviation value for LED source.  $\sigma$  in the histogram represents the standard deviation of the optical path length 67

Fig 5.8 Temporal stability of the system. Histogram represents the measured counts for thickness fluctuation at each spatial point (standard deviation of time varying thickness). The mean of these values represents the temporal stability of the microscope. Inset shows the time varying thickness at one spatial point. 67

Fig 5.9 Reconstructed wrapped phase distribution of polystyrene beads (b) continuous phase distribution obtained after phase unwrapping (c) thickness profile (d) line profile of the thickness distribution. LED source ( $\lambda=627\text{nm}$ ) is used to illuminate the sample. 68

Fig 5.10 Quantitative phase imaging of human erythrocytes using LED source and multiplexed holograms (a) recorded multiplexed hologram (b) quantitative phase imaging corresponding to the two fields of views marked in Fig 5.10a(c) 3D rendering of thickness distribution of RBCs inside the area of interest marked by white rectangle (d) cross sectional thickness profile of the RBC along the dashed line marked in Fig 5.10b 69

Fig 5.11 Quantitative phase imaging of human erythrocytes using UV LED and multiplexed holograms (a) Portion of the recorded multiplexed hologram (b) 3D rendering of thickness distribution of RBCs 70

Fig 5.12 Improvement in lateral resolution at shorter wavelengths (a) and (b) portions of recorded hologram showing line structure of Group 7 element 6 of the resolution target using 627nm and 385nm LED sources respectively. (c) and (d) represent the reconstructed intensity patterns for 627nm and 385nm LED sources (e) line profile of the intensity variation 70

Fig 5.13 3D printed Fresnel biprism device with optical and imaging components (b) dimensions of the setup (c) device in working mode 71

Fig 5.14 A typical Lloyd's mirror interferometer 72

Fig 5.15 (a) Large field of view wavefront division digital holographic interference microscope employing Lloyd's mirror configuration. (b) Interference of modulated and un-modulated portion of the laser beam leading to creation of holograms (c) and (d) table top version of the microscope in the laboratory 73

Fig 5.16 (a) Dimensions of the field portable 3D printed microscope (b) 3D printed module attached with a mobile phone through OTG cable (Video 2 shows the working of the 3D printed device employing Lloyd's mirror) 74

Fig 5.17 Temporal stability of the system. Histogram represents the measured counts for thickness fluctuation at each spatial point (standard deviation of time varying thickness). The mean of these values represents the temporal stability of the microscope. Inset shows the time varying thickness at a spatial point in the field of view. 75

Fig 5.18 Reconstructed phase distribution in the case where (a) the object is introduced in the path of the entire laser beam and (b) the object was introduced in a portion on the

illuminating laser beam. The overlap of images from the direct beam and the beam folded on to the sensor by the mirror can be seen (inside the dashed rectangle). 76

Fig 5.19 Microscope calibration using 15 $\mu$ m diameter polystyrene microspheres. (a) Wrapped phase distribution obtained after phase subtraction (b) Continuous phase distribution obtained after phase unwrapping. (c) Thickness distribution of the microsphere. (d) Cross-sectional profile of the thickness distribution. 77

Fig 5.20 Quantitative phase imaging of red blood cell distributions. (a) Recorded hologram of a dense distribution red blood cell (b) Continuous phase distribution obtained after phase subtraction. (c) Thickness distribution computed from the continuous phase distribution. 78

Fig 5.21 shows the 3D schematic of the common path self-referencing digital holographic interference microscope employing Lloyd's mirror interferometer and LED (b) shows the table top setup in the laboratory 79

Fig 5.22 (a) recorded hologram of polystyrene beads (b) continuous phase distribution obtained after unwrapping (c) thickness distribution of the Polystyrene beads (d) line profile of the polystyrene bead 80

Fig 5.23 Quantitative phase imaging of human erythrocytes using LED source and Lloyd's mirror (a) recorded hologram (b) continuous phase distribution of the recorded RBCs (a) (c) 3D rendering of thickness distribution of RBCs inside the area of interest marked by white rectangle (d) cross sectional thickness profile of the RBC along the dashed line marked in Fig 5.23 (b) 81

Fig 5.24 A typical Sagnac interferometer 82

Fig 5.25 2D schematic of the common path self-referencing digital holographic microscope employing He-Ne laser and Sagnac interferometer 83

Fig 5.26 (a) recorded hologram of polystyrene beads (b) continuous phase distribution obtained after unwrapping (c) thickness distribution of the Polystyrene beads (d) line profile of the polystyrene bead 83

Fig 5.27 Quantitative phase imaging of human erythrocytes using He-Ne laser and Sagnac interferometer (a) recorded hologram (b) continuous phase distribution of the recorded RBCs (a) (c) 3D rendering of thickness distribution of RBCs inside the area of interest marked by white rectangle (d) cross sectional thickness profile of the RBC along the dashed line marked in Fig 5.27 (b) 84

Fig 5.28 (a) shows the 3D schematic of the common path self-referencing digital holographic interference microscope employing Sagnac interferometer and LED (b) shows the table top setup in the laboratory 85

Fig 5.29 Temporal stability of the system. Histogram represents the measured counts for thickness fluctuation at each spatial point (standard deviation of time varying thickness). The

mean of these values represents the temporal stability of the microscope. Inset shows the time varying thickness for a spatial point in the FOV. 86

Fig 5.30 (a) recorded hologram of polystyrene beads (b) continuous phase distribution obtained after unwrapping (c) thickness distribution of the Polystyrene beads (d) line profile of the polystyrene bead 87

Fig 5.31 Quantitative phase imaging of human erythrocytes using LED and Sagnac interferometer (a) recorded hologram (b) continuous phase distribution of the recorded RBCs (c) 3D rendering of thickness distribution of RBC (d) cross sectional thickness profile of the RBC along the dashed line marked in Fig 5.31b. 88

Fig 6.1 (a) The hologram recording from the beams after passing through shearing (b) Unfolding of the interference pattern formation in the off-axis Lens-less digital holographic microscope 93

Fig 6.2 Schematic of the Lens-less off axis common path DHIM based on lateral shearing interferometer employing laser diode 96

Fig 6.3 (a) 3D schematic of the developed lens less microscope employing lateral shearing interferometer and a laser diode module (b) Photograph of the lens-less microscope in the lab. 96

Fig 6.4 Temporal stability of the system. Histogram represents the measured counts for thickness fluctuation at spatial points (standard deviation of time varying thickness). The mean of these values represents the temporal stability of the device. Inset shows the time varying thickness at a spatial point in the field of view. 97

Fig 6. 5 (a) Hologram of the USAF target (b) interference fringes in the marked yellow box in 6.5a 98

Fig 6.6 (a) to (c) Numerical focusing (a) inside best focus, (b) at best focus (c) outside best focus. (d) Numerically reconstructed wrapped phase distribution at the best focus plane. (e) Digitally subtracted spherical phase factor. (f) Object phase obtained after digital phase compensation. 98

Fig 6.7 (a) Hologram of ink dots on microscope slide (b) Interference fringes inside the region of interest (c) reconstructed intensity at the best focus plane 99

Fig 6.8 (a) Hologram of numbers written on a microscope slide using a marker pen (b) Reconstructed Intensity profile (c) Reconstructed Phase distribution profile (d) Object phase after subtraction of spherical phase (e) Object phase after unwrapping and tilt phase subtraction (f) Three-dimensional rendering of object phase distribution 100

Fig 6.11 (a) hologram of the USAF target recorded using the lens-less microscope using LED source and a pair of Fresnel biprisms (b) reconstructed continuous phase distribution at the best focus plane (c) the 3D rendering of the spatially varying object phase distribution 102

Fig 7.1 General OCT system based on a Michelson interferometer	107
Fig 7.2 Schematic of the developed FDOCT system	112
Fig 7.3 Experimental setup of FDOCT	112
Fig 7.4 Spectrum of the LED source used in the experiments	112
Fig 7.5 (a) Recorded spectral interference pattern for 10 $\mu$ m path length delay between object and reference paths (b) Intensity profile along the line shown in Fig. 7.5a	114
Fig 7.6 Recorded spectral interference patterns at different axial positions of the scanning mirror and the reconstructed depth profiles by Fourier Transforming the intensity profile along each column	115
Fig 7.7 Fourier transform of the spectral intensity patterns along the line shown in Fig. 7.6. Each Fourier transform represents 10 $\mu$ m translation of the scanning mirror.	115
Fig 7.8 (a) Recorded spectral interference pattern with two axially separated mirrors as object. (b) Reconstructed intensity profile at various axial positions. (c) Intensity profile in the plane represented by the dashed rectangle in Fig. 7.8b, showing the positions of the two mirrors.	117
Fig 7.9 (a) Spectral interference pattern for two axially separated mirrors as object. (b) Fourier transform of the spectral interference pattern of the intensity variation along the red line providing depth information about Mirror 1. (c) Fourier transform of the intensity variation along the blue line providing depth information about Mirror 2.	118
Fig 7.10 (a) Recorded interference patterns for different lateral positions of the scanning beam (a) reflection only from the back coated mirror. (b) reflection from back coated mirror and the first mirror behind it. (c) reflection from back coated mirror and second mirror behind it. (d) to (e) Fourier transform of the intensity variation along the lines shown in Fig. 7.10 (a) to (c) respectively.	119
Fig 7.11 Reconstructed intensity from the Fourier transforms of the interference pattern for each lateral position of the scanning beam. (a) at depth 32 $\mu$ m (b) at depth 58 $\mu$ m (c) at depth 74 $\mu$ m (d) at depth 87 $\mu$ m (e) at depth 103 $\mu$ m, and (f) at depth 140 $\mu$ m. (g) Variation in reflected light intensity with depth	120
Fig 7.12 Reflected intensity with depth (a) along the dashed red line in Fig. 7.11b. (c) along the dashed blue line in Fig. 7.11b	121

## **Executive summary**

Observation is the first and one of the most fundamental steps in scientific methodology. In the field of biomedical imaging, for observing and accessing information, light microscopy is still one of the least invasive and widely used technique. Brightfield light microscopes have several features that make them ideal for imaging biological cells, including high lateral resolution which matches the size of the sub-cellular structures of the cells. It is also relatively non-perturbing in nature enabling one to study the biological cells for a longer period to follow their dynamics. However, brightfield light microscopes only provide two-dimensional information about the sample (cells) under investigation. Moreover, such microscopes provide only low contrast images since most biological cells are transparent to visible light. Contrast is improved by staining the sample (chemical processing), which may deteriorate its life cycle. Hence, techniques that would provide high contrast images of low absorbing samples along with their thickness information without the need of staining (labelling) would be highly useful. The thickness information could provide knowledge about the state of the health of the cell under investigation, leading to its characterization and classification. The advancement in laser technology and digital sensors along with holography, extended the horizon of imaging techniques. Due to this evolution, the field of biomedical imaging has witnessed immense growth but there are still many low and middle-income countries that face major shortages of imaging equipment and diagnostic tools which becomes an obstacle for quick and affordable diagnosis and treatment of several diseases. Moreover, most of the present-day diagnostic tools are required to be operated under stringent conditions, by trained technicians. Therefore, the design and development of tools that are rugged, stand-alone, compact, inexpensive as well as field deployable, requiring minimum human intervention is essential to address these issues.

The work described in this thesis, details the efforts that has been made to investigate interferometric as well non interferometric techniques for the three-dimensional imaging of technical and biological samples using low coherent light emitting diodes (LEDs). The developed techniques can image and provide, bio-physical and bio-mechanical parameters of samples including human erythrocytes (red blood cells - RBCs), which will be useful in examining them for their characterization. LEDs offer certain advantages over laser such as they are small, rugged, bright, cost effective, and have a longer lifetime. Moreover, LEDs being low temporally coherent, minimizes the effect of speckles and parasitic interference patterns, which otherwise acts as a noise in the resulting images. These features of LEDs acted as a driving force to use them as an alternative to laser in the developed imaging devices. The use

of LEDs has also cut down the form factor and the cost of the developed systems. However, owing to their low spatiotemporal coherence, it becomes difficult to use LEDs in interferometric techniques as it does not generate high contrast interference fringes across a significant area (field of view). To tackle this issue, a sincere effort has been put forward to incorporate LEDs in interferometric techniques by means of special optical arrangement and geometries for performing quantitative phase contrast imaging. Furthermore, the investigated designs of digital holographic microscopes (interference microscopes) involving Lloyd's mirror and Fresnel Biprism have been converted into field portable, cost-effective devices using off the shelf components and 3D printing of the microscope structure. These devices can be used for point-of-care cell characterization, leading to assessment of the sample health. Apart from harnessing the low coherent property of LED, its intensity has also been exploited for retrieving phase information through Fringe projection technique (non-interferometric technique). Further, a Fourier domain optical coherence tomography (FDOCT) system have been developed by utilizing LED as the light source to obtain sample depth information. The technique is demonstrated as a proof of concept that a sufficiently high-power LED can be used as an alternative to super luminescent diodes which are conventionally used to perform OCT by making the system compact and cost-effective. The use of low-end CMOS sensors (Webcam) as a detector, further reduced the cost of the system.

## **Chapter 1: Introduction**

Chapter 1 puts forward an introduction and overview to the problem that is addressed in this thesis. It provides a brief of the techniques involved in the work and a short discussion and introduction to each technique including their pros and cons. Non interferometric and interferometric techniques have been discussed which have been implemented to perform quantitative phase contrast imaging of RBCs. A lens-less technique has also been discussed which has been employed to reduce the aberration that arise due to lens and other optical components. FDOCT has also been performed utilizing LED instead of the conventional light source used which is the superluminescent diode in order to make the system cost effective.

## Chapter 2: Coherence

Chapter 2 discusses about the fundamental and inherent property of the light source; coherence, which has a particularly important implication in imaging systems. Broadly speaking, coherence has two aspects associated to it, one that focuses on the correlation of a wave with itself at different time points is termed as temporal coherence whereas the one that represents the mutual coherence of different parts of the same wavefront termed as spatial coherence. The chapter describes both temporal and spatial coherence and how the use of laser (high coherent source) poses some limitations in the imaging system by degrading the image quality (due to speckle noise). It also discusses several advantages of utilizing LED (low coherent) as an alternative to laser in interferometric as well as non-interferometric techniques which are digital holographic microscopy and fringe projection technique respectively.

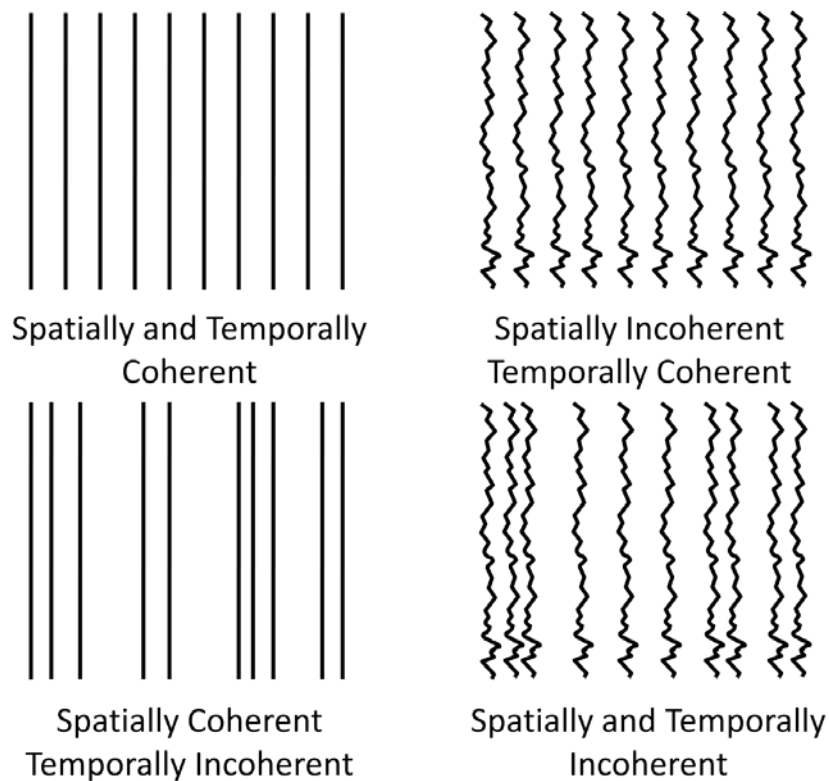


Fig 2. 1 Pictorial representation of temporal and spatial coherence in the case of plane waves

### Chapter 3: Fringe Projection Technique

Chapter 3 focuses on the implementation of a non-interferometric, non-invasive technique for generating three-dimensional surface information namely Fringe projection technique which is made up of a projection unit, image acquisition unit and a processing unit. In this technique, a structured pattern (sinusoidal or grid pattern) is projected on the object under investigation. Depth information is encoded in the deformed pattern which is imaged by the digital sensor array. This technique can be used in two modes: reflection and transmission. The study focuses on shape measurement of optical components such as wedges, cylindrical rods and cylindrical lens etc. Further the technique is also implemented to retrieve three-dimensional information of human RBCs.

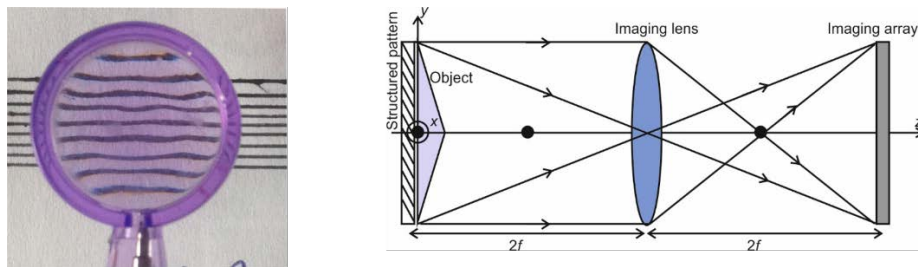


Fig 3.1 Recorded modulation of line pattern projected through a lens and optical system configuration for imaging the structured pattern projected through object under investigation. A magnification of 1 is used in the simulations

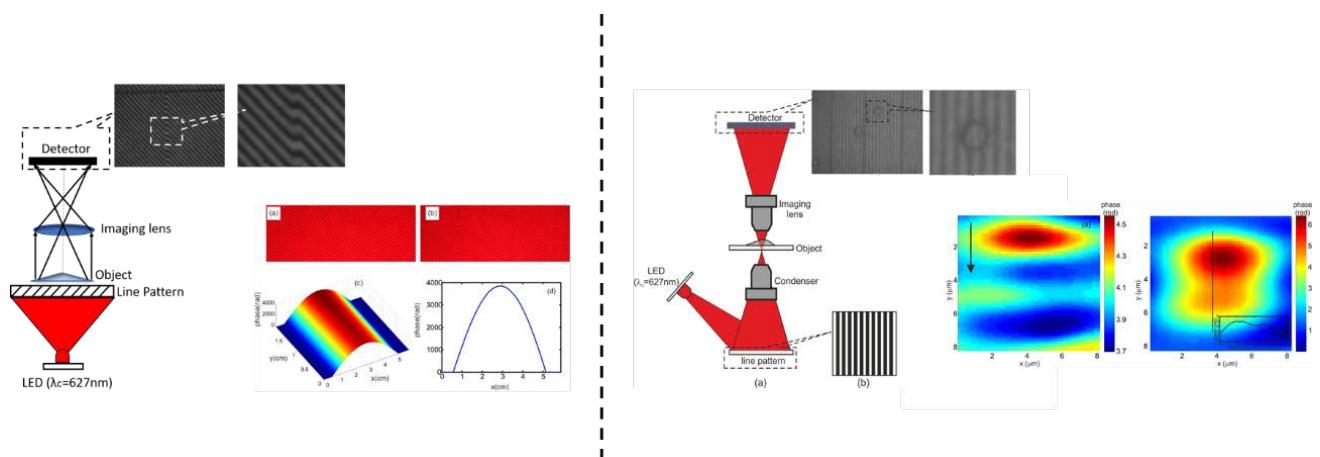


Fig 3.2 Schematic of the Fringe projection technique for the measurement of phase objects (Cylindrical glass rod and human red blood cells) and their respective results obtained.

## Chapter 4: Theory of holography

Chapter 4 explains the theory behind the recording and reconstruction of holograms. It also describes the mathematical formulation related to the angular spectrum propagation approach of the scalar diffraction theory and Fourier fringe analysis that is used to analyse the recorded data.

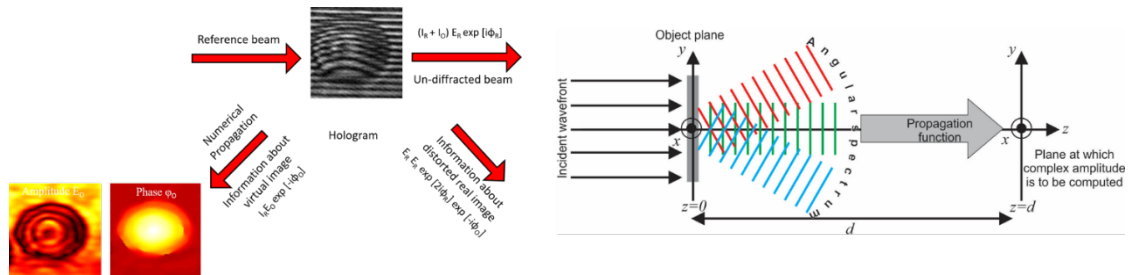


Fig 4.1 Digital hologram reconstruction. Reference wave gets scattered from the structures of the hologram. It is numerically propagated to the position where the object existed (virtual image) and Numerical reconstruction of digital holograms using ASP approach

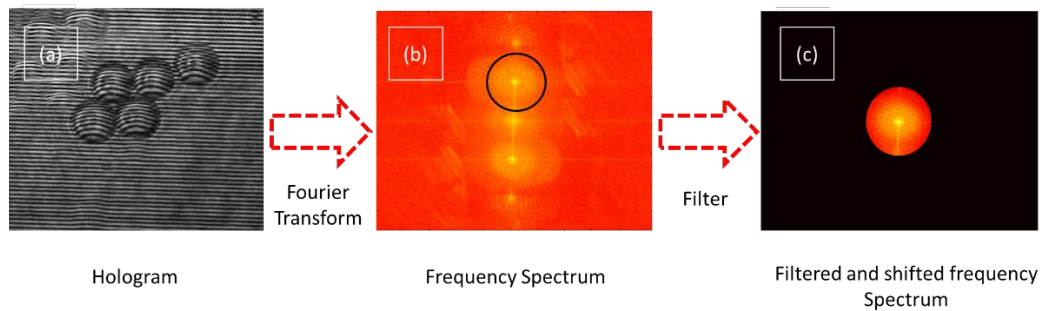


Fig 4.2 Hologram illuminated by the reference wavefront. (b) Power spectrum of the hologram obtained after Fourier transform, where three components (un-diffracted reference, real object and virtual object) can be seen. (c) Filtered spectrum, which contains only the spatial frequencies corresponding to object alone. This is then propagated to the image plane

## Chapter 5: Wide field of view common path self-referencing digital holographic microscopy employing LED

Chapter 5 describes how low coherent source such as LED is integrated as a light source in various common path self-referencing geometries to perform quantitative phase contrast imaging of human RBCs. The coherence properties of LED are exploited in order to generate high contrast interference fringes over a large FOV. Common path self-referencing configuration such as Sagnac, Lloyd's mirror and Fresnel biprism have been explored to harness the coherence of LED employing it for performing digital holography microscopy. The work also includes increasing the effective FOV by hologram multiplexing. The use of exotic wavelength such as UV LED has also been explored for performing the experiment in so as to enhance the resolution of the system. The chapter also includes designing and development of 3D printed, stand alone, portable and cost-effective device based on Lloyd's mirror interferometer and Fresnel Biprism interferometer. A comparative study has also been undertaken using the above-mentioned geometries and with a combination of different sources and sensors.

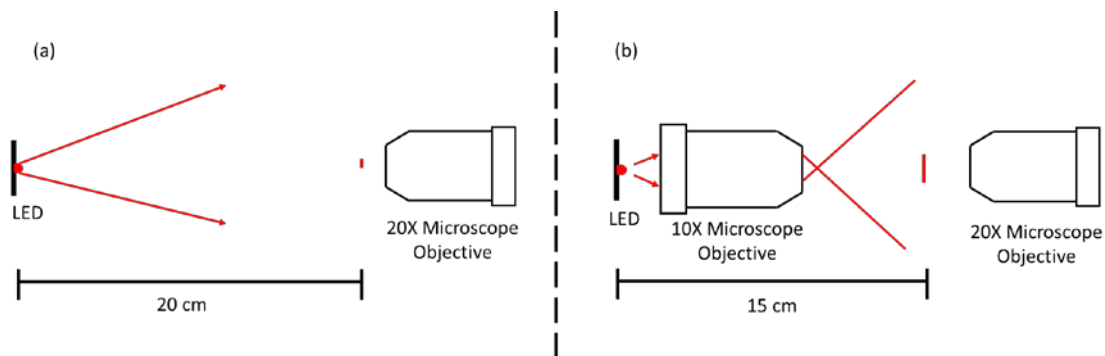


Fig 5.1 Diameter of the spatial coherence area increases upon demagnifying the light emitting area of the source.

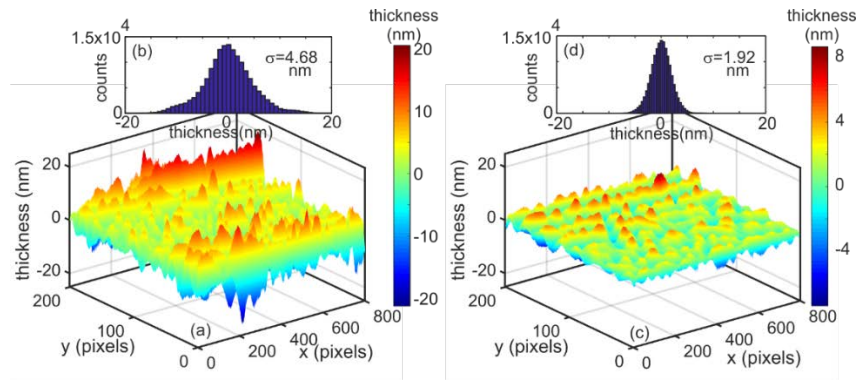


Fig 5.2 Spatial stability (a) spatially varying optical path length using laser source (b) histogram of the spatial thickness variation along with the standard computed standard deviation value for laser source. (c) spatially varying thickness using LED source (d) histogram of the spatial thickness along with the standard computed standard deviation value for LED source.  $\sigma$  in the histogram represents the standard deviation of the optical path length

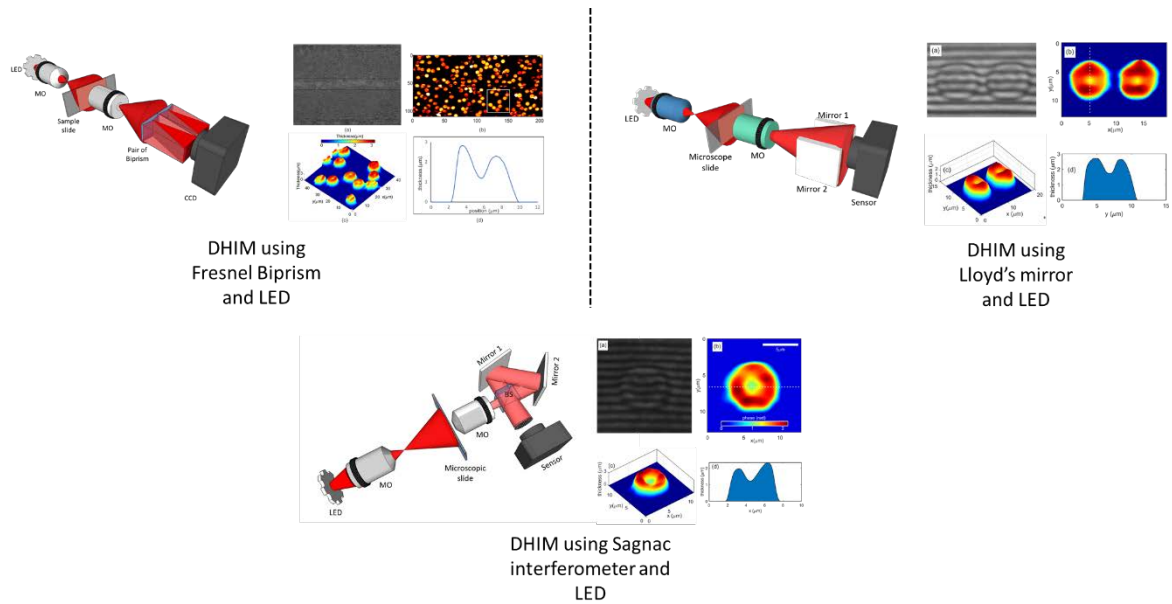


Fig 5.3 Self-referencing common path configurations and the results obtained: Fresnel Biprism interferometer, Lloyd's mirror and Sagnac interferometer that were implemented to perform digital holographic microscopy to obtain 3D images of human red blood cells utilizing LED as the light source

## Chapter 6: Large field of view self-referencing lens-less Holographic Microscopy

Chapter 6 describes the application of lens-less imaging techniques. To attain high-resolution imaging, lenses are necessary nevertheless lens-less imaging is serviceable where high resolution is not a major requirement. A lens-less digital holographic microscope is developed to examine micro- objects by employing lateral shearing interferometer. Furthermore, the lens-less system would make the microscope compact, easy to implement, portable, robust, and also eliminate the aberration introduces due to a lens.

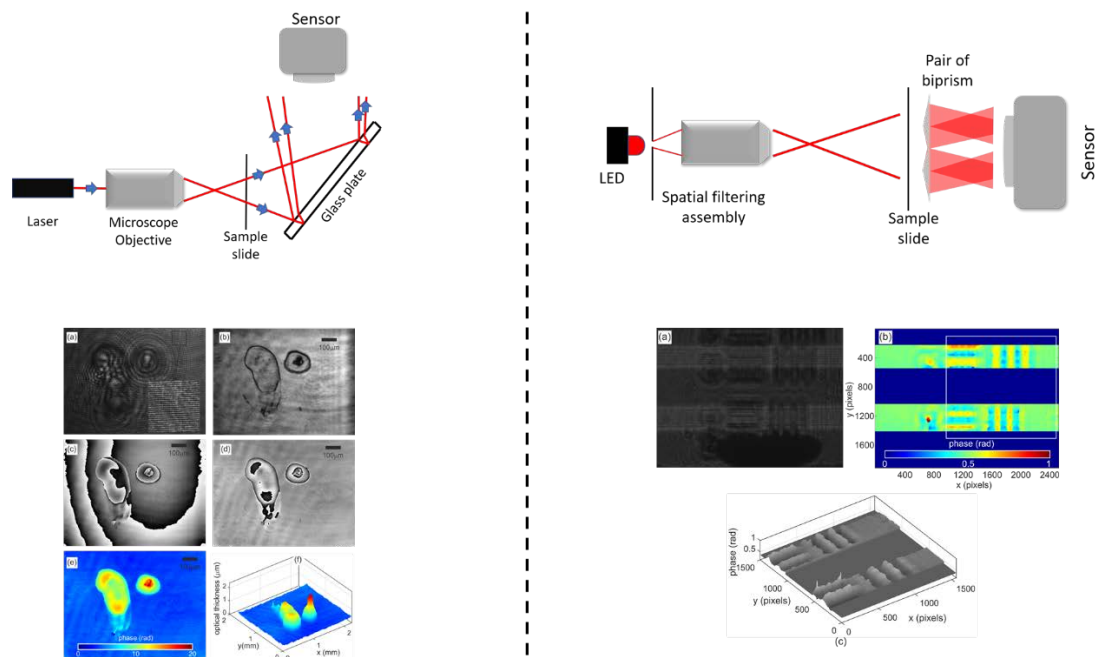


Fig 6.1 Schematics and results obtained by implementing lens-less digital holographic microscopy to obtain phase images of technical objects such as USAF and numbers written on a microscope slide using a marker pen using Laser with lateral shearing interferometer and LED with a pair of Fresnel Biprism interferometer

## Chapter 7: Low-cost Optical Coherence Tomographic System using LEDs

Chapter 7 introduces the theory of Optical coherence tomography (OCT) which is a rapidly emerging, robust, non-invasive, three-dimensional sub surface tissue imaging technique. In this chapter design of a cost-effective Fourier Domain Optical Coherence Tomography (FD-OCT) system which employs an LED source is describes. The LED source offers features such as relative simplicity, compactness, robustness. Moreover, LEDs are low cost, unlike Super luminescent Diode (SLD) which is the standard light source used in commercially available OCT devices. The developed design uses a Webcam instead of a high-end detector to record the data. Theoretical formulation of Time domain OCT and Fourier Domain OCT has also been discussed in this chapter.

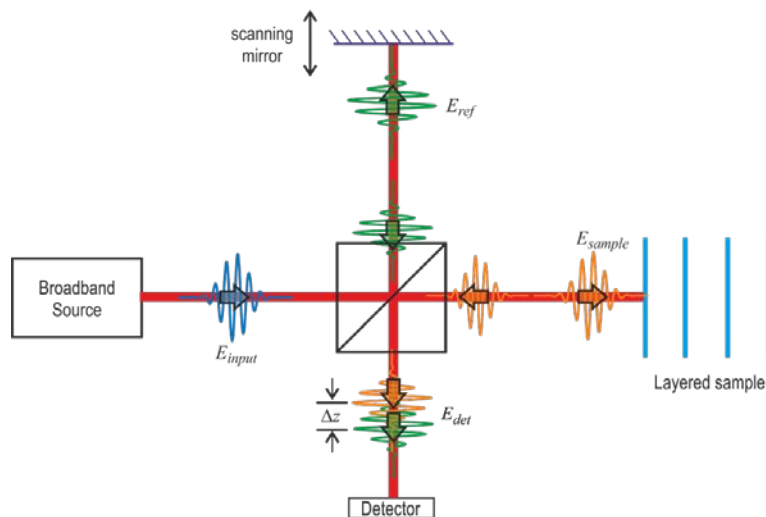


Fig 7.1 General OCT system based on a Michelson interferometer

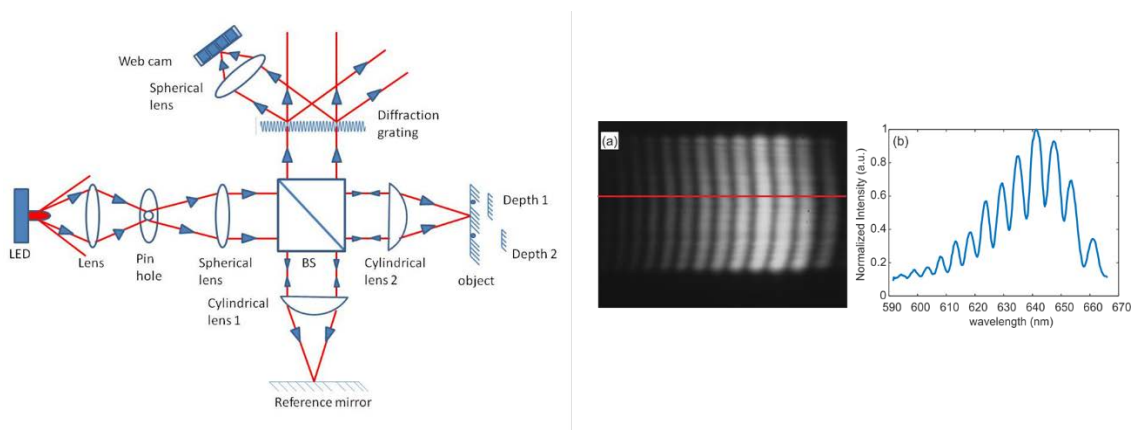


Fig 7.2 Schematic of the developed low-cost FD-OCT system and Recorded spectral interference pattern for 10mm path length delay between object and reference paths, intensity profile along the line shown in (a)

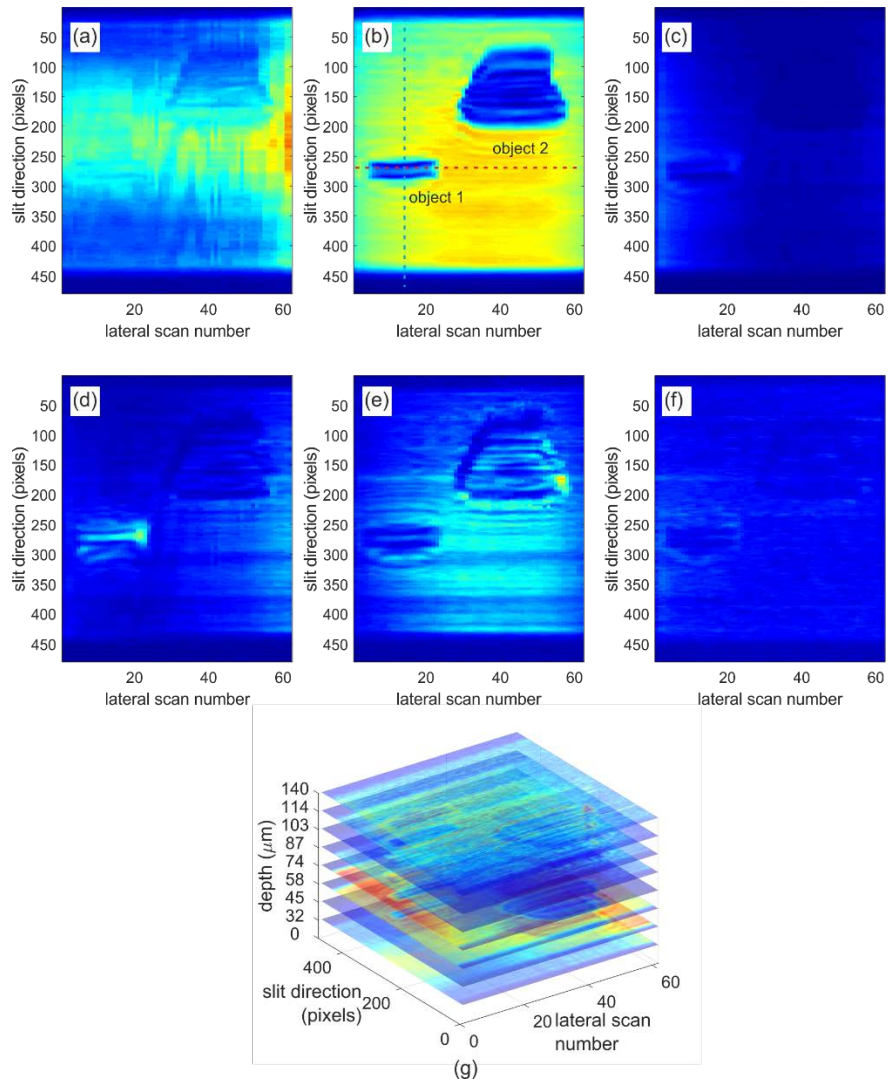


Fig 7.2 Reconstructed intensity from the Fourier transforms of the interference pattern for each lateral position of the scanning beam. (a) at depth 32mm (b) at depth 58mm (c) at depth 74mm (d) at depth 87mm (e) at depth 103mm, and (f) at depth 140mm. (g) Variation in reflected light intensity with depth

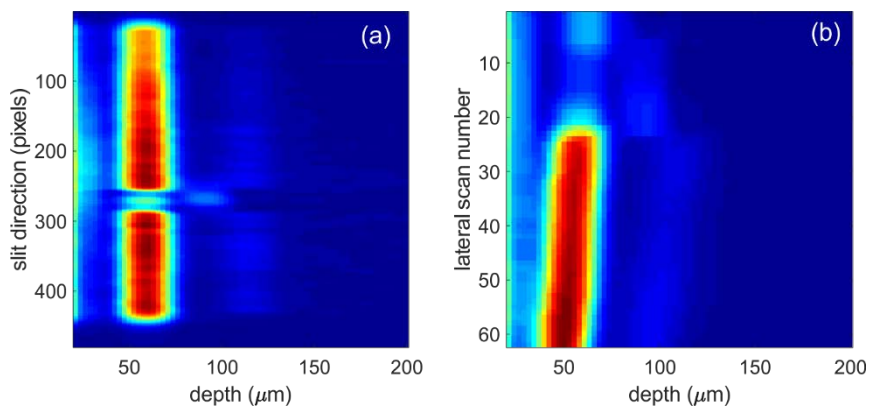


Fig 7.3 Reflected intensity with depth (a) along the dashed red line in Fig. 7.2 b. (b) along the dashed blue line in Fig. 7.2 b

## References:

1. Z. Sun, K. H. Ng, and N. Ramli, "Biomedical imaging research: a fast-emerging area for interdisciplinary collaboration," *Biomed Imaging Interv. J.* **7**(3), e21 (2011).
2. G. Popescu, *Quantitative Phase Imaging of Cells and Tissues* (New York: McGraw-Hill, 2011).
3. B. Crosson, A. Ford, K. M. McGregor, M. Meinzer, S. Cheshkov, L. Xiufeng, D. Walker-Batson, and R. W. Briggs, "Functional imaging and related techniques: An introduction for rehabilitation researchers," *J. Rehabil. Res. Dev.* (2010).
4. W. W. Orrison, "Introduction to Brain Imaging," in *Functional Brain Imaging* (1995).
5. R. Salzer and H. W. Siesler, *Infrared and Raman Spectroscopic Imaging* (2009).
6. G. D. Luker and K. E. Luker, "Optical imaging: Current applications and future directions," *J. Nucl. Med.* (2008).
7. D. J. Brady, *Optical Imaging and Spectroscopy* (John Wiley & Sons, Inc., 2009).
8. C. M. C. Tempany, "Advances in Biomedical Imaging," *JAMA* **285**(5), 562 (2001).
9. R. L. Ehman, W. R. Hendee, M. J. Welch, N. R. Dunnick, L. B. Bresolin, R. L. Arenson, S. Baum, H. Hricak, and J. H. Thrall, "Blueprint for Imaging in Biomedical Research," *Radiology* **244**(1), 12–27 (2007).
10. F. Pesapane, M. Codari, and F. Sardanelli, "Artificial intelligence in medical imaging: threat or opportunity? Radiologists again at the forefront of innovation in medicine," *Eur. Radiol. Exp.* (2018).
11. W. M. Report, *World Malaria Report 2017. Geneva: World Health Organization* (2017).
12. World Health Organization, *Global Tuberculosis Report* (2015).
13. A. Trampuz, M. Jereb, I. Muzlovic, and R. M. Prabhu, "Clinical review: Severe malaria," *Crit. Care* **7**, (2003).
14. *World Malaria Report 2020* (2020).
15. J. L. Miller, "Iron Deficiency Anemia: A Common and Curable Disease," *Cold Spring Harb. Perspect. Med.* **3**(7), a011866–a011866 (2013).
16. World Health Organization, "Conclusions and recommendations of the WHO Consultation on prevention and control of iron deficiency in infants and young children in malaria-endemic areas.," *Food Nutr. Bull.* **28**(4 Suppl), S621-7 (2007).
17. E. McLean, M. Cogswell, I. Egli, D. Wojdyla, and B. de Benoist, "Worldwide

- prevalence of anaemia, WHO Vitamin and Mineral Nutrition Information System, 1993–2005," *Public Health Nutr.* **12**(04), 444 (2009).
18. D. Jamison, J. Breman, A. Measham, G. Alleyne, M. Claeson, D. Evans, P. Jha, A. Mills, and P. Musgrove, *Disease Control Priorities in Developing Countries*, 2nd Edition (2006).
  19. B. Czaja, M. Gutierrez, G. Závodszy, D. de Kanter, A. Hoekstra, and O. Eniola-Adefeso, "The influence of red blood cell deformability on hematocrit profiles and platelet margination," *PLOS Comput. Biol.* **16**(3), e1007716 (2020).
  20. S. Suresh, J. Spatz, J. P. Mills, A. Micoulet, M. Dao, C. T. Lim, M. Beil, and T. Seufferlein, "Connections between single-cell biomechanics and human disease states: gastrointestinal cancer and malaria," *Acta Biomater.* **1**(1), 15–30 (2005).
  21. V. K. Katiyar and D. Fisseha, "Analysis of Mechanical Behavior of Red Blood Cell Membrane with Malaria Infection," *World J. Mech.* **01**(03), 100–108 (2011).
  22. B. Javidi, A. Markman, S. Rawat, T. O'Connor, A. Anand, and B. Andemariam, "Sickle cell disease diagnosis based on spatio-temporal cell dynamics analysis using 3D printed shearing digital holographic microscopy," *Opt. Express* **26**(10), 13614 (2018).
  23. N. R. Patel, V. K. Chhaniwal, B. Javidi, and A. Anand, "Identification of malaria infected red blood samples by digital holographic quantitative phase microscope," in *Optics InfoBase Conference Papers*, E. Beaufort, P. T. C. So, F. Pavone, and E. M. Hillman, eds. (2015), p. 95360E.
  24. G. Tomaiuolo, "Biomechanical properties of red blood cells in health and disease towards microfluidics," *Biomicrofluidics* **8**(5), 051501 (2014).
  25. M. Diez-Silva, M. Dao, J. Han, C.-T. Lim, and S. Suresh, "Shape and Biomechanical Characteristics of Human Red Blood Cells in Health and Disease.," *MRS Bull.* **35**(5), 382–388 (2010).
  26. N. T. Shaked, L. L. Satterwhite, M. J. Telen, G. A. Truskey, and A. Wax, "Quantitative microscopy and nanoscopy of sickle red blood cells performed by wide field digital interferometry," *J. Biomed. Opt.* **16**(3), 030506 (2011).
  27. S. Tuvia, S. Levin, A. Bitler, and R. Korenstein, "Mechanical fluctuations of the membrane-skeleton are dependent on F-actin ATPase in human erythrocytes.," *J. Cell Biol.* **141**(7), 1551–61 (1998).
  28. S. Lee, H. Park, S. Jang, and P. Yongkeun, "Refractive Index Tomograms and Dynamic Membrane Fluctuations of Red Blood Cells from Patients with Diabetes Mellitus," *Blood* **128**(22), (2016).
  29. J. Tapia, N. Vera, J. Aguilar, M. González, S. A. Sánchez, P. Coelho, C. Saavedra, and J. Staforelli, "Correlated flickering of erythrocytes membrane observed with dual time resolved membrane fluctuation spectroscopy under different d-glucose concentrations," *Sci. Rep.* **11**(1), 2429 (2021).

30. N. S. Gov and S. A. Safran, "Red Blood Cell Membrane Fluctuations and Shape Controlled by ATP-Induced Cytoskeletal Defects," *Biophys. J.* **88**(3), 1859–1874 (2005).
31. Y. Park, C. A. Best, K. Badizadegan, R. R. Dasari, M. S. Feld, T. Kuriabova, M. L. Henle, A. J. Levine, and G. Popescu, "Measurement of red blood cell mechanics during morphological changes," *Proc. Natl. Acad. Sci.* **107**(15), 6731–6736 (2010).
32. R. Huisjes, A. Bogdanova, W. W. van Solinge, R. M. Schiffelers, L. Kaestner, and R. van Wijk, "Squeezing for Life – Properties of Red Blood Cell Deformability," *Front. Physiol.* **9**, (2018).
33. F. Brochard and J. F. Lennon, "Frequency spectrum of the flicker phenomenon in erythrocytes," *J. Phys.* **36**(11), 1035–1047 (1975).
34. G. Bao and S. Suresh, "Cell and molecular mechanics of biological materials," *Nat. Mater.* (2003).
35. G. Popescu, K. Badizadegan, R. R. Dasari, and M. S. Feld, "Observation of dynamic subdomains in red blood cells," *J. Biomed. Opt.* (2006).
36. H. Turlier, D. A. Fedosov, B. Audoly, T. Auth, N. S. Gov, C. Sykes, J. F. Joanny, G. Gompper, and T. Betz, "Equilibrium physics breakdown reveals the active nature of red blood cell flickering," *Nat. Phys.* (2016).
37. G. Popescu, T. Ikeda, K. Goda, C. A. Best-Popescu, M. Laposata, S. Manley, R. R. Dasari, K. Badizadegan, and M. S. Feld, "Optical Measurement of Cell Membrane Tension," *Phys. Rev. Lett.* **97**(21), 218101 (2006).
38. W. Choi, J. Yi, and Y. W. Kim, "Fluctuations of red blood cell membranes: The role of the cytoskeleton," *Phys. Rev. E* **92**(1), 012717 (2015).
39. J. Evans, W. Gratzner, N. Mohandas, K. Parker, and J. Sleep, "Fluctuations of the Red Blood Cell Membrane: Relation to Mechanical Properties and Lack of ATP Dependence," *Biophys. J.* **94**(10), 4134–4144 (2008).
40. D. B. Murphy, "Fundamentals of light microscopy and Electronic imaging," in *John Wiley and Sons. Inc* (2001), **83**(991).
41. D. B. Murphy and M. W. Davidson, *Fundamentals of Light Microscopy and Electronic Imaging* (John Wiley & Sons, Inc., 2012).
42. K. Thorn, "A quick guide to light microscopy in cell biology," *Mol. Biol. Cell* **27**(2), 219–222 (2016).
43. D. J. Stephens and V. J. Allan, "Light microscopy techniques for live cell imaging.," *Science* **300**(5616), 82–6 (2003).
44. G. Wang and N. Fang, "Imaging and Spectroscopic Analysis of Living Cells," *Sci.*

Direct (2012).

45. H. A. Alturkistani, F. M. Tashkandi, and Z. M. Mohammedsaleh, "Histological Stains: A Literature Review and Case Study," *Glob. J. Health Sci.* **8**(3), 72 (2015).
46. R. L. Price and W. Gray (Jay) Jerome, "More Basic Confocal Microscopy: A Tutorial," *Microsc. Microanal.* **9**(S02), 1568–1569 (2003).
47. J. Jonkman, C. M. Brown, G. D. Wright, K. I. Anderson, and A. J. North, "Tutorial: guidance for quantitative confocal microscopy," *Nat. Protoc.* **15**(5), 1585–1611 (2020).
48. A. Ettinger and T. Wittmann, "Fluorescence live cell imaging," in *Methods in Cell Biology* (2014), **123**, pp. 77–94.
49. U. Kubitscheck, *Fluorescence Microscopy: From Principles to Biological Applications* (2013).
50. F. Zernike, "Phase contrast, a new method for the microscopic observation of transparent objects," *Physica* **9**(7), 686–698 (1942).
51. C. J. Mann, L. Yu, C.-M. Lo, and M. K. Kim, "High-resolution quantitative phase-contrast microscopy by digital holography," *Opt. Express* **13**(22), 8693 (2005).
52. A. Arun and B. Javidi, "Digital holographic microscopy for automated 3D cell identification: an overview (Invited Paper)," *Chinese Opt. Lett.* **12**(6), 060012–060017 (2014).
53. B. Kemper and G. von Bally, "Digital holographic microscopy for live cell applications and technical inspection," *Appl. Opt.* **47**(4), A52 (2008).
54. A. Anand, V. Chhaniwal, and B. Javidi, "Tutorial: Common path self-referencing digital holographic microscopy," *APL Photonics* **3**(7), (2018).
55. B. Kemper, A. Bauwens, A. Vollmer, S. Ketelhut, P. Langehanenberg, J. Müthing, H. Karch, and G. von Bally, "Label-free quantitative cell division monitoring of endothelial cells by digital holographic microscopy," *J. Biomed. Opt.* **15**(3), 036009 (2010).
56. A. Anand and B. Javidi, "Digital holographic microscopy for automated 3D cell identification: an overview," *Chinese Opt. Lett.* **12**(6), 10–15 (2014).
57. A. Anand, A. Faridian, V. K. Chhaniwal, S. Mahajan, V. Trivedi, S. K. Dubey, G. Pedrini, W. Osten, and B. Javidi, "Single beam Fourier transform digital holographic quantitative phase microscopy," *Appl. Phys. Lett.* **104**(10), 1–6 (2014).
58. E. CuChe, F. Bevilacqua, and C. Depeursinge, "Digital holography for quantitative phase-contrast imaging," *Opt. Lett.* **24**(5), 291 (1999).
59. A. Anand, V. K. Chhaniwal, and B. Javidi, "Real-time digital holographic microscopy

- for phase contrast 3D imaging of dynamic phenomena," *IEEE/OSA J. Disp. Technol.* **6**(10), 500–505 (2010).
60. S. Ebrahimi, M. Dashtdar, E. Sánchez-Ortiga, M. Martínez-Corral, and B. Javidi, "Stable and simple quantitative phase-contrast imaging by Fresnel biprism," *Appl. Phys. Lett.* **112**(11), 113701 (2018).
  61. P. V Vora, "Development Of 3D Techniques For Phase Contrast Imaging Of Micro Objects," The M. S. University of Baroda (2017).
  62. A. Anand, P. Vora, S. Mahajan, V. Trivedi, V. Chhaniwal, A. Singh, R. Leitgeb, and B. Javidi, "Compact, common path quantitative phase microscopic techniques for imaging cell dynamics," *Pramana* **82**(1), 71–78 (2014).
  63. P. Marquet, B. Rappaz, P. J. Magistretti, E. Cuche, Y. Emery, T. Colomb, and C. Depeursinge, "Digital holographic microscopy: a noninvasive contrast imaging technique allowing quantitative visualization of living cells with subwavelength axial accuracy," *Opt. Lett.* **30**(5), 468 (2005).
  64. S. Mahajan, V. Trivedi, P. Vora, V. Chhaniwal, B. Javidi, and A. Anand, "Highly stable digital holographic microscope using Sagnac interferometer," *Opt. Lett.* **40**(16), 3743 (2015).
  65. A. S. G. Singh, A. Anand, R. A. Leitgeb, and B. Javidi, "Lateral shearing digital holographic imaging of small biological specimens," *Opt. Express* **20**(21), 23617 (2012).
  66. U. Schnars and W. P. O. J ptner, "Digital recording and numerical reconstruction of holograms," *Meas. Sci. Technol.* **13**(9), R85–R101 (2002).
  67. U. Schnars and W. Jueptner, *Digital Holography* (Springer-Verlag, 2005).
  68. W. Osten, A. Faridian, P. Gao, K. Körner, D. Naik, G. Pedrini, A. K. Singh, M. Takeda, and M. Wilke, "Recent advances in digital holography [Invited]," *Appl. Opt.* **53**(27), G44 (2014).
  69. A. Anand, I. Moon, and B. Javidi, "Automated Disease Identification With 3-D Optical Imaging: A Medical Diagnostic Tool," *Proc. IEEE* **105**(5), 924–946 (2017).
  70. B. Javidi, S. Yeom, I. Moon, and M. Daneshpanah, "Real-time automated 3D sensing, detection, and recognition of dynamic biological micro-organic events," *Opt. Express* **14**(9), 3806 (2006).
  71. B. Javidi, I. Moon, and M. Daneshpanah, "3D imaging, visualization, and recognition of biological micro-organisms," in *Three-Dimensional TV, Video, and Display V*, B. Javidi, F. Okano, and J.-Y. Son, eds. (2006), p. 639202.
  72. K. Alm, Z. El-Schich, M. Falck, A. Gjrloff Wingren, B. Janicke, and S. Oredsso, "Cells and Holograms – Holograms and Digital Holographic Microscopy as a Tool to Study the Morphology of Living Cells," in *Holography - Basic Principles and Contemporary*

*Applications* (InTech, 2013), (May).

73. A. Faridian, D. Hopp, G. Pedrini, U. Eigenthaler, M. Hirscher, and W. Osten, "Nanoscale imaging using deep ultraviolet digital holographic microscopy," *Opt. Express* **18**(13), 14159 (2010).
74. B. Javidi, M. Daneshpanah, I. Moon, S. Bagheri, and A. Anand, "3-D Identification and Tracking of Biological Microorganisms Using Computational Microscopy," in *Digital Holography and Three-Dimensional Imaging* (2010).
75. J. Garcia-Sucerquia, "Partially coherent lensless holographic microscopy with micrometre resolution applied to extended objects," *3D Res.* **2**(2), 2 (2011).
76. I. Moon and B. Javidi, "Three-dimensional identification of stem cells by computational holographic imaging," *J. R. Soc. Interface* **4**(13), 305–313 (2007).
77. S. Amann, M. von Witzleben, and S. Breuer, "3D-printable portable open-source platform for low-cost lens-less holographic cellular imaging," *Sci. Rep.* **9**(1), 11260 (2019).
78. A. Anand, V. K. Chhaniwal, N. R. Patel, and B. Javidi, "Automatic identification of malaria-infected RBC with digital holographic microscopy using correlation algorithms," *IEEE Photonics J.* **4**(5), 1456–1464 (2012).
79. N. T. Shaked, "Quantitative phase microscopy of biological samples using a portable interferometer," *Opt. Lett.* **37**(11), 2016 (2012).
80. V. Chhaniwal, A. S. G. Singh, R. A. Leitgeb, B. Javidi, and A. Anand, "Quantitative phase-contrast imaging with compact digital holographic microscope employing Lloyd's mirror," *Opt. Lett.* **37**(24), 5127 (2012).
81. W. Zhang, L. Cao, R. Li, H. Zhang, H. Zhang, Q. Jiang, and G. Jin, "Wavefront division digital holography," *AIP Adv.* **8**(5), 055304 (2018).
82. N. Patel, V. Trivedi, S. Mahajan, V. Chhaniwal, C. Fournier, S. Lee, B. Javidi, and A. Anand, "Wavefront division digital holographic microscopy," *Biomed. Opt. Express* (2018).
83. N. Patel, S. Rawat, M. Joglekar, V. Chhaniwal, S. K. Dubey, T. O'Connor, B. Javidi, and A. Anand, "Compact and low-cost instrument for digital holographic microscopy of immobilized micro-particles," *Opt. Lasers Eng.* **137**, 106397 (2021).
84. P. Vora and A. Anand, "Wide field of view common-path lateral-shearing digital holographic interference microscope," *J. Biomed. Opt.* **22**(12), 1 (2017).
85. D. GABOR, "A New Microscopic Principle," *Nature* **161**(4098), 777–778 (1948).
86. D. Gabor, "Microscopy by reconstructe dwavefronts," *Proc. R. Soc. London. Ser. A. Math. Phys. Sci.* **197**, 454–87 (1949).

87. D. Gabor, "Microscopy by Reconstructed Wave Fronts: II," *Proc. Phys. Soc. Sect. B* **64**(6), 449–469 (1951).
88. V. Pourreza Ghoushchi, M. Aas, E. Ulusoy, and H. Ürey, "Effect of spatial coherence of LED sources on image resolution in holographic displays," in *Advances in Display Technologies VII* (2017).
89. T.-C. Poon, *Digital Holography and Three-Dimensional Display* (Springer US, 2006).
90. T. Latychevskaia and H.-W. Fink, "Solution to the Twin Image Problem in Holography," *Phys. Rev. Lett.* **98**(23), 233901 (2007).
91. E. N. Leith and J. Upatnieks, "Reconstructed Wavefronts and Communication Theory," *J. Opt. Soc. Am.* **52**(10), 1123 (1962).
92. E. N. Leith and J. Upatnieks, "Wavefront Reconstruction with Diffused Illumination and Three-Dimensional Objects," *J. Opt. Soc. Am.* **54**(11), 1295 (1964).
93. P. Petruck, R. Riesenberger, and R. Kowarschik, "Optimized coherence parameters for high-resolution holographic microscopy," *Appl. Phys. B Lasers Opt.* **106**(2), 339–348 (2012).
94. J. Garcia-Sucerquia, "Noise reduction in digital lensless holographic microscopy by engineering the light from a light-emitting diode," *Appl. Opt.* **52**(1), A232 (2013).
95. V. Bianco, P. Memmolo, M. Leo, S. Montresor, C. Distanto, M. Paturzo, P. Picart, B. Javidi, and P. Ferraro, "Strategies for reducing speckle noise in digital holography," *Light Sci. Appl.* **7**(1), 48 (2018).
96. F. Pan, L. Yang, and W. Xiao, "Coherent noise reduction in digital holographic microscopy by averaging multiple holograms recorded with a multimode laser," *Opt. Express* **25**(18), 21815 (2017).
97. S. Kosmeier, P. Langehanenberg, G. von Bally, and B. Kemper, "Reduction of parasitic interferences in digital holographic microscopy by numerically decreased coherence length," *Appl. Phys. B* **106**(1), 107–115 (2012).
98. Y. Deng and D. Chu, "Coherence properties of different light sources and their effect on the image sharpness and speckle of holographic displays," *Sci. Rep.* (2017).
99. J.-P. Liu, T. Tahara, Y. Hayasaki, and T.-C. Poon, "Incoherent Digital Holography: A Review," *Appl. Sci.* **8**(1), 143 (2018).
100. R. Guo, F. Wang, X. Hu, and W. Yang, "Off-axis low coherence digital holographic interferometry for quantitative phase imaging with an LED," *J. Opt. (United Kingdom)* (2017).
101. J. W. Goodman, *Speckle Phenomena in Optics: Theory and Applications, Second Edition* (2020).

102. M. Ott, "Capabilities and reliability of LEDs and laser diodes," Technol. Valid. Assur. Group, Swales Aerospace, Compon. Technol. Radiat. Eff. Branch NASA Goddard Sp. Flight Cent. (1997).
103. F. Dubois, N. Callens, C. Yourassowsky, M. Hoyos, P. Kurowski, and O. Monnom, "Digital holographic microscopy with reduced spatial coherence for three-dimensional particle flow analysis," *Appl. Opt.* **45**(5), 864–871 (2006).
104. G. Li, Y. Qiu, and H. Li, "Coherence theory of a laser beam passing through a moving diffuser," *Opt. Express* **21**(11), 13032 (2013).
105. T. Stangner, H. Zhang, T. Dahlberg, K. Wiklund, and M. Andersson, "Step-by-step guide to reduce spatial coherence of laser light using a rotating ground glass diffuser," *Appl. Opt.* **56**(19), 5427 (2017).
106. M. Tziraki, R. Jones, P. M. W. French, M. R. Melloch, and D. D. Nolte, "Photorefractive holography for imaging through turbid media using low coherence light," *Appl. Phys. B Lasers Opt.* (2000).
107. F. Dubois, M. L. N. Requena, C. Minetti, O. Monnom, and E. Istasse, "Partial spatial coherence effects in digital holographic microscopy with a laser source," *Appl. Opt.* **43**(5), 1131–1139 (2004).
108. M. C. Pitter, C. W. See, and M. G. Somekh, "Full-field heterodyne interference microscope with spatially incoherent illumination," *Opt. Lett.* (2004).
109. Y. Park, W. Choi, Z. Yaqoob, R. Dasari, K. Badizadegan, and M. S. Feld, "Speckle-field digital holographic microscopy," *Opt. Express* (2009).
110. Y. Choi, T. D. Yang, K. J. Lee, and W. Choi, "Full-field and single-shot quantitative phase microscopy using dynamic speckle illumination," *Opt. Lett.* (2011).
111. B. Redding, M. A. Choma, and H. Cao, "Speckle-free laser imaging using random laser illumination," *Nat. Photonics* (2012).
112. K. Lee, H.-D. Kim, K. Kim, Y. Kim, T. R. Hillman, B. Min, and Y. Park, "Synthetic Fourier transform light scattering," *Opt. Express* (2013).
113. D. Alvarez-Palacio and J. Garcia-Sucerquia, "Digital in-line holographic microscopy with partially coherent light: Micrometer resolution," *Rev. Mex. Fis.* (2010).
114. R. Guo, B. Yao, J. Min, M. Zhou, X. Yu, M. Lei, S. Yan, Y. Yang, and D. Dan, "LED-based digital holographic microscopy with slightly off-axis interferometry," *J. Opt. (United Kingdom)* (2014).
115. R. Guo, B. Yao, P. Gao, J. Min, M. Zhou, J. Han, X. Yu, X. Yu, M. Lei, S. Yan, Y. Yang, D. Dan, and T. Ye, "Off-axis digital holographic microscopy with LED illumination based on polarization filtering," *Appl. Opt.* (2013).

116. B. Kemper, S. Stürwald, C. Remmersmann, P. Langehanenberg, and G. von Bally, "Characterisation of light emitting diodes (LEDs) for application in digital holographic microscopy for inspection of micro and nanostructured surfaces," *Opt. Lasers Eng.* **46**(7), 499–507 (2008).
117. J. Garcia-Sucerquia, "White-light light-emitting diode to simplify color digital lensless holographic microscopy," in *2012 11th Euro-American Workshop on Information Optics, WIO 2012* (2012).
118. F. Dubois and C. Yourassowsky, "Off-axis multispectral digital holographic microscope with partially coherent illumination," in *Optical Modelling and Design II* (2012).
119. T. Yamauchi, H. Iwai, M. Miwa, and Y. Yamashita, "Low-coherent quantitative phase microscope for nanometer-scale measurement of living cells morphology," *Opt. Express* (2008).
120. O. Mudanyali, D. Tseng, C. Oh, S. O. Isikman, I. Sencan, W. Bishara, C. Oztoprak, S. Seo, B. Khademhosseini, and A. Ozcan, "Compact, light-weight and cost-effective microscope based on lensless incoherent holography for telemedicine applications," *Lab Chip* (2010).
121. F. Dubois and C. Yourassowsky, "Full off-axis red-green-blue digital holographic microscope with LED illumination," *Opt. Lett.* **37**(12), 2190 (2012).
122. S. Stürwald, B. Kemper, C. Remmersmann, P. Langehanenberg, and G. von Bally, "Application of light emitting diodes in digital holographic microscopy," in *Optical Micro- and Nanometrology in Microsystems Technology II*, C. Gorecki, A. K. Asundi, and W. Osten, eds. (2008), p. 699507.
123. M. Joglekar, V. Trivedi, R. Bhatt, V. Chhaniwal, S. Dubey, D. Claus, G. Pedrini, R. Leitgeb, B. Javidi, and A. Anand, "Compact, low cost, large field-of-view self-referencing digital holographic interference microscope," *Optik (Stuttg.)* **245**(May), 167615 (2021).
124. V. Singh, S. Tayal, and D. S. Mehta, "Highly stable wide-field common path digital holographic microscope based on a Fresnel biprism interferometer," *OSA Contin.* **1**(1), 48 (2018).
125. S. Rawat, S. Komatsu, A. Markman, A. Anand, and B. Javidi, "Compact and field-portable 3D printed shearing digital holographic microscope for automated cell identification," *Appl. Opt.* **56**(9), D127 (2017).
126. A. Anand, M. Joglekar, H. Shah, V. Trivedi, S. Mahajan, V. Chhaniwal, R. Leitgeb, and B. Javidi, "Imaging the effect of hemoglobin on properties of RBCs using common-path digital holographic microscope," in *Advances in Microscopic Imaging*, F. S. Pavone, E. Beaufort, and P. T. So, eds. (SPIE, 2017), **Part F61-E**, p. 19.
127. P. Girshovitz and N. T. Shaked, "Doubling the field of view in off-axis low-coherence interferometric imaging," *Light Sci. Appl.* **3**(3), e151–e151 (2014).

128. P. Girshovitz, I. Frenklach, and N. T. Shaked, "Broadband quantitative phase microscopy with extended field of view using off-axis interferometric multiplexing," *J. Biomed. Opt.* **20**(11), 1 (2015).
129. P. S. Huang and F.-P. Chiang, "Recent advances in fringe projection technique for 3D shape measurement," in *SHE Conference on Optical Diagnostics for Fluids/Heat/Combustion and Photomechanics for Solids*, S. S. Cha, P. J. Bryanston-Cross, and C. R. Mercer, eds. (1999), pp. 132–142.
130. A. Li, X. Peng, Y. Yin, X. Liu, Q. Zhao, K. Körner, and W. Osten, "Fringe projection based quantitative 3D microscopy," *Optik (Stuttg.)*. (2013).
131. S. S. Gorthi and P. Rastogi, "Fringe projection techniques: Whither we are?," *Opt. Lasers Eng.* **48**(2), 133–140 (2010).
132. B. Dessus and M. Leblanc, "The "fringe method" and its application to the measurement of deformations, vibrations, contour lines and differences of objects," *Opto-electronics* (1973).
133. E. Mueller, "Fast three-dimensional form measurement system," *Opt. Eng.* **34**(9), 2754 (1995).
134. G. Sansoni, S. Corini, S. Lazzari, R. Rodella, and F. Docchio, "Three-dimensional imaging based on Gray-code light projection: characterization of the measuring algorithm and development of a measuring system for industrial applications," *Appl. Opt.* **36**(19), 4463 (1997).
135. A. C. Sobieranski, F. Inci, H. C. Tekin, M. Yuksekkaya, E. Comunello, D. Cobra, A. von Wangenheim, and U. Demirci, "Portable lensless wide-field microscopy imaging platform based on digital inline holography and multi-frame pixel super-resolution," *Light Sci. Appl.* **4**(10), e346–e346 (2015).
136. L. Orzo, B. Wittner, and S. Tokes, "High speed water monitoring systems based on Digital Holographic Microscopy," in *CSIT 2013 - 9th International Conference on Computer Science and Information Technologies, Revised Selected Papers* (2013).
137. Y. Wu and A. Ozcan, "Lensless digital holographic microscopy and its applications in biomedicine and environmental monitoring," *Methods* **136**, 4–16 (2018).
138. A. Ozcan and E. McLeod, "Lensless Imaging and Sensing," *Annu. Rev. Biomed. Eng.* **18**(1), 77–102 (2016).
139. R. Corman, W. Boutu, A. Campalans, P. Radicella, J. Duarte, M. Kholodtsova, L. Bally-Cuif, N. Dray, F. Harms, G. Dovillaire, S. Bucourt, and H. Merdji, "Lensless microscopy platform for single cell and tissue visualization," *Biomed. Opt. Express* (2020).
140. S. Shin and Y. Yu, "Lensless Reflection Digital Holographic Microscope with a Fresnel-Bluestein Transform," *J. Korean Phys. Soc.* **74**(2), 98–101 (2019).

141. M. N. Gurcan, L. E. Boucheron, A. Can, A. Madabhushi, N. M. Rajpoot, and B. Yener, "Histopathological Image Analysis: A Review," *IEEE Rev. Biomed. Eng.* (2009).
142. A. Bohr and K. Memarzadeh, "The rise of artificial intelligence in healthcare applications," in *Artificial Intelligence in Healthcare* (Elsevier, 2020), pp. 25–60.
143. S. Aime, A. Alberich, A. Almen, O. Arthurs, H. Barthel, O. Clément, M. Crean, N. de Souza, F. Demuth, M. Dewey, V. Dousset, A. Frangi, C. Garos, X. Golay, P. Gordebeke, M. Günther, H. Hahn, M. Hierath, C. Hoeschen, M. Hunink, H. U. Kauczor, G. Krestin, K. Krischak, G. Langs, Y. Liu, L. Marti-Bonmati, C. Matos, U. Mayerhofer-Sebera, J. McNulty, K. Muylle, M. Neeman, W. Niessen, K. Nikolaou, P. Pereira, A. Persson, A. Pifferi, K. Riklund, A. Rockall, K. Rosendahl, F. Sardanelli, S. Sourbron, O. Speck, V. Valentini, and P. Zolda, "Strategic research agenda for biomedical imaging," *Insights Imaging* (2019).
144. O. Maiques, M. Georgouli, and V. Sanz-Moreno, "Recent advances in tissue imaging for cancer research," *F1000Research* **8**, 1980 (2019).
145. E. Gupta, P. Bhalla, N. Khurana, and T. Singh, "Histopathology for the Diagnosis of infectious diseases," *Indian J. Med. Microbiol.* **27**(2), 100–106 (2009).
146. W. Jung and S. A. Boppart, "Optical coherence tomography for rapid tissue screening and directed histological sectioning," *Anal. Cell. Pathol.* (2012).
147. W. Jung and S. A. Boppart, "Modern Trends in Imaging V: Optical Coherence Tomography for Rapid Tissue Screening and Directed Histological Sectioning," *Anal. Cell. Pathol.* **35**(3), 129–143 (2012).
148. T. Peters, *Image-Guided Interventions: Technology and Applications* (Springer, 2008).
149. J. T. Yap, J. P. J. Carney, N. C. Hall, and D. W. Townsend, "Image-guided cancer therapy using PET/CT," *Cancer J.* (2004).
150. T. Tjardes, S. Shafizadeh, D. Rixen, T. Paffrath, B. Bouillon, E. S. Steinhausen, and H. Baethis, "Image-guided spine surgery: State of the art and future directions," *Eur. Spine J.* (2010).
151. R. R. Alfano, S. G. Demos, and S. K. Gayen, "Advances in optical imaging of biomedical media," *Ann. N. Y. Acad. Sci.* **820**(112), 248–271 (1997).
152. C. Dunsby and P. M. W. French, "Techniques for depth-resolved imaging through turbid media including coherence-gated imaging," *J. Phys. D. Appl. Phys.* **36**(14), R207–R227 (2003).
153. J. G. Fujimoto, "Optical coherence tomography," *Comptes Rendus l'Academie des Sci. - Ser. IV Physics, Astrophys.* **2**(8), 1099–1111 (2001).
154. B. Bouma, ed., *Handbook of Optical Coherence Tomography* (CRC Press, 2001).

155. R. Bernardes and J. Cunha-Vaz, eds., *Optical Coherence Tomography*, Biological and Medical Physics, Biomedical Engineering (Springer Berlin Heidelberg, 2012).
156. Y. Verma, "Biomedical imaging using optical coherence tomography," Homi Bhabha National Institute (2012).
157. X. Yu, J. Hong, C. Liu, and M. K. Kim, "Review of digital holographic microscopy for three-dimensional profiling and tracking," *Opt. Eng.* **53**(11), 112306 (2014).
158. J. C. Hebden, S. R. Arridge, and D. T. Delpy, "Optical imaging in medicine: I. Experimental techniques," *Phys. Med. Biol.* **42**(5), 825–840 (1997).
159. P. H. Tomlins and R. K. Wang, "Theory, developments and applications of optical coherence tomography," *J. Phys. D. Appl. Phys.* **38**(15), 2519–2535 (2005).
160. S. A. Boppart, "Optical coherence tomography: Technology and applications for neuroimaging," *Psychophysiology* **40**(4), 529–541 (2003).
161. T. Bernas, D. Barnes, E. K. Asem, J. P. Robinson, and B. Rajwa, "Precision of light intensity measurement in biological optical microscopy," *J. Microsc.* (2007).
162. D. Malacara, *Optical Shop Testing: Third Edition* (2006).
163. S. Sridhar and A. Da Silva, "Enhanced contrast and depth resolution in polarization imaging using elliptically polarized light," *J. Biomed. Opt.* (2016).
164. P. S. Considine, "Effects of Coherence on Imaging Systems\*," *J. Opt. Soc. Am.* (1966).
165. S. K. Narayanan and R. S. D. Wahidabanu, "A View on Despeckling in Ultrasound Imaging," *Int. J. Signal Process. Image Process. Pattern Recognit.* (2009).
166. E. Wolf, "Non-cosmological redshifts of spectral lines," *Nature* (1987).
167. J. . Dainty, *Laser Speckle and Related Phenomenon* (Springer-Verlag Berlin Heidelberg, 1975).
168. P. F. W. Osten, "Optical inspection of microsystems," in *Optical Inspection of Microsystems* (CRC Taylor and Francis, 2007).
169. S. Inoué, *Video Microscopy* (Springer US, 1986).
170. R. Erf, *Speckle Metrology* (Elsevier, 1978).
171. D. Malacara, M. Servín, and Z. Malacara, *Interferogram Analysis for Optical Testing* (CRC Press, 2018).
172. T. Kreis, *Handbook of Holographic Interferometry* (Wiley, 2004).
173. J. M. Schmitt, S. H. Xiang, and K. M. Yung, "Speckle in Optical Coherence

- Tomography," *J. Biomed. Opt.* **4**(1), 95 (1999).
174. K. R. Lee, K. Kim, J. Jung, J. H. Heo, S. Cho, S. Lee, G. Chang, Y. J. Jo, H. Park, and Y. K. Park, "Quantitative phase imaging techniques for the study of cell pathophysiology: From principles to applications," *Sensors (Switzerland)* (2013).
  175. K. Kim, J. Yoon, S. Shin, S. Lee, S.-A. Yang, and Y. Park, "Optical diffraction tomography techniques for the study of cell pathophysiology," *J. Biomed. Photonics Eng.* (2016).
  176. S. Shin, Y. Kim, K. Lee, K. Kim, Y.-J. Kim, H. Park, and Y. Park, "Common-path diffraction optical tomography with a low-coherence illumination for reducing speckle noise," in *Quantitative Phase Imaging* (2015).
  177. B. E. A. Saleh and M. C. Teich, "Fundamentals of Photonics , 2nd Edition," Wiley (2007).
  178. E. Wolf, *Introduction to the Theory of Coherence and Polarization of Light*, 1st editio (Cambridge University Press, 2007).
  179. A. Ahmad, T. Mahanty, V. Dubey, A. Butola, B. S. Ahluwalia, and D. S. Mehta, "Effect on the longitudinal coherence properties of a pseudothermal light source as a function of source size and temporal coherence," *Opt. Lett.* (2019).
  180. J. W. Goodman, "Introduction to Fourier Optics," in *Mc-Graw Hill* (McGraw-Hill, 1968).
  181. W. Lauterborn, T. Kurz, and M. Wiesenfeldt, *Coherent Optics -Fundamentals and Applications* (Springer, 1993).
  182. T. Kreis, *Handbook of Holographic Interferometry* (2004).
  183. S. Shin, K. Kim, K. Lee, S. Lee, and Y. Park, "Effects of spatiotemporal coherence on interferometric microscopy," *Opt. Express* (2017).
  184. M. Francon, *Diffraction: Coherence in Optics* (Pergamon, 2013).
  185. W. Albrecht, *Physik von Laser Und Maser* (Bibliographisches Institut Manheim, 1984).
  186. H. S. Nalwa and L. S. Rohwer, *Handbook of Luminescence Display Materials and Devices* (ASP Press, California, 2003).
  187. E. F. Schubert, *Light-Emitting Diodes* (Cambridge University Press, 2006).
  188. D. S. Mehta, K. Saxena, S. K. Dubey, and C. Shakher, "Coherence characteristics of light-emitting diodes," *J. Lumin.* (2010).
  189. S. W. Sanderson and K. L. Simons, "Light emitting diodes and the lighting revolution: The Emergence of a solid-state lighting industry," *Res. Policy* (2014).

190. S. Nakamura, T. Mukai, and M. Senoh, "Candela-class high-brightness InGaN/AlGaIn double-heterostructure blue-light-emitting diodes," *Appl. Phys. Lett.* (1994).
191. Y. Narukawa, "White-Light LEDs," *Opt. Photonics News* (2004).
192. R. S. Sirohi, *Introduction to OPTICAL METROLOGY* (CRC Press, 2017).
193. K. J. Gåsvik, *Optical Metrology* (Wiley, 2002).
194. S. Zhang, "Handbook of 3D Machine Vision: Optical Metrology and Imaging," in *Handbook of 3D Machine Vision: Optical Metrology and Imaging* (2013).
195. O. D. D. Soares, *Optical Metrology* (Springer Netherlands, 1987).
196. T. Yoshizawa, *Handbook of Optical Metrology: Principles and Applications, Second Edition* (2015).
197. B. H. Walker, "Optical Metrology Applications In The Testing Of Military Optical Systems," in *Proceedings Volume 0416, Applications of Optical Metrology: Techniques and Measurements II*, J. J. Lee, ed. (1983), pp. 37–42.
198. M. A. Beeck and W. Hentschel, "Laser metrology - a diagnostic tool in automotive development processes," *Opt. Lasers Eng.* (2000).
199. M. Vaez-Iravani, "Optical Inspection and Metrology in Semiconductor Manufacturing," in (2013).
200. J. M. Saint Clair, "Challenges for optical metrology in the aerospace industry," in *Optics InfoBase Conference Papers* (2014).
201. S. Zhang, "Recent progresses on real-time 3D shape measurement using digital fringe projection techniques," *Opt. Lasers Eng.* **48**(2), 149–158 (2010).
202. S. Hsu, S. Acharya, A. Rafii, and R. New, "Performance of a time-of-flight range camera for intelligent vehicle safety applications," in *Advanced Microsystems for Automotive Applications 2006* (2006).
203. G. M. Brown, "Overview of three-dimensional shape measurement using optical methods," *Opt. Eng.* (2000).
204. P. Hariharan, "Basics of holography," in *Cambridge University Press* (2012), **66**, pp. 37–39.
205. P. K. Rastogi, ed., *Holographic Interferometry*, Springer Series in Optical Sciences (Springer Berlin Heidelberg, 1994), **68**.
206. A. E. Ennos, "Speckle Interferometry," in (1975), pp. 203–253.
207. R. Jones and C. Wykes, *Holographic and Speckle Interferometry* (1989).

208. P. Jacquot and J.-M. Fournier, eds., *Interferometry in Speckle Light* (Springer Berlin Heidelberg, 2000).
209. D. Post, "Developments In Moire Interferometry," *Opt. Eng.* (1982).
210. A. C. Walker, *Handbook of Moire Measurement* (CRC Press, 2019).
211. K. Ramesh, ed., *Digital Photoelasticity* (Springer Berlin Heidelberg, 2000).
212. Y. Jain, "Stress Analysis Using Photoelasticity Technique – A Review," *Int. J. Res. Appl. Sci. Eng. Technol.* (2017).
213. D. Malacara, *Optical Shop Testing: Third Edition* (2006).
214. J. Sanderson, *Understanding Light Microscopy* (2019).
215. L. C. Chen and C. C. Huang, "Miniaturized 3D surface profilometer using digital fringe projection," *Meas. Sci. Technol.* (2005).
216. K. Genovese and C. Pappalettere, "Whole 3D shape reconstruction of vascular segments under pressure via fringe projection techniques," *Opt. Lasers Eng.* **44**(12), 1311–1323 (2006).
217. F. Lilley, "Robust fringe analysis system for human body shape measurement," *Opt. Eng.* (2000).
218. C. J. Moore, D. R. Burton, O. Skydan, P. J. Sharrock, and M. Lalor, "3D body surface measurement and display in radiotherapy part I: Technology of structured light surface sensing," in *Proceedings - International Conference on Medical Information Visualisation - BioMedical Visualisation, MediVis 2006* (2006).
219. A. Hanafi, T. Gharbi, and J. Y. Cornu, "In vivo measurement of lower back deformations with Fourier-transform profilometry," *Appl. Opt.* (2005).
220. F. Berryman, P. Pynsent, J. Fairbank, and S. Disney, "A new system for measuring three-dimensional back shape in scoliosis," *Eur. Spine J.* (2008).
221. T. Hain, R. Eckhardt, K. Kunzi-Rapp, and B. Schmitz, "Indications for Optical Shape Measurements in Orthopaedics and Dermatology," *Med. Laser Appl.* **17**(1), 55–58 (2002).
222. Y. Ferrag, D. Black, J. M. Lagarde, A. M. Schmitt, S. Dahan, J. L. Grolleau, and S. Mordon, "Use of a 3-D imaging technique for non-invasive monitoring of the depth of experimentally induced wounds," *Ski. Res. Technol.* (2007).
223. S. Jaspers, H. Hopermann, G. Sauermann, U. Hoppe, R. Lunderstädt, and J. Ennen, "Rapid in vivo measurement of the topography of human skin by active image triangulation using a digital micromirror device," *Ski. Res. Technol.* **5**(3), 195–207 (1999).

224. J. M. Lagarde, C. Rouvrais, D. Black, S. Diridollou, and Y. Gall, "Skin topography measurement by interference fringe projection: A technical validation," *Ski. Res. Technol.* (2001).
225. C. Quan, C. J. Tay, X. Y. He, X. Kang, and H. M. Shang, "Microscopic surface contouring by fringe projection method," *Opt. Laser Technol.* (2002).
226. X. Y. He, W. Sun, X. Zheng, and M. Nie, "Static and Dynamic Deformation Measurements of Micro Beams by the Technique of Digital Image Correlation," *Key Eng. Mater.* (2006).
227. S. T. Yilmaz, U. D. Özüğürel, K. Bulut, and M. N. Inci, "Vibration amplitude analysis with a single frame using a structured light pattern of a four-core optical fibre," *Opt. Commun.* (2005).
228. Q. Zhang and X. Su, "High-speed optical measurement for the drumhead vibration," *Opt. Express* (2005).
229. M. de Angelis, S. De Nicola, P. Ferraro, A. Finizio, and G. Pierattini, "Liquid refractometer based on interferometric fringe projection," *Opt. Commun.* **175**(4–6), 315–321 (2000).
230. Q. C. Zhang and X. Y. Su, "An optical measurement of vortex shape at a free surface," *Opt. Laser Technol.* (2002).
231. P. J. Cobelli, A. Maurel, V. Pagneux, and P. Petitjeans, "Global measurement of water waves by Fourier transform profilometry," *Exp. Fluids* (2009).
232. P. . Huang, F. Jin, and F.-P. Chiang, "Quantitative evaluation of corrosion by a digital fringe projection technique," *Opt. Lasers Eng.* **31**(5), 371–380 (1999).
233. P.-R. Jang, R. Arunkumar, T. Leone, Z. Long, M. A. Mott, O. P. Norton, W. P. Okhuysen, Y. Su, D. L. Monts, P. G. Kirk, and J. Ettien, "Quantitative imaging characterization of aluminum pit corrosion in Oak Ridge research reactor pool," in *Advanced Environmental, Chemical, and Biological Sensing Technologies IV*, T. Vo-Dinh, R. A. Lieberman, and G. Gauglitz, eds. (2006), p. 63770S.
234. G. S. Spagnolo and D. Ambrosini, "Diffractive optical element based sensor for roughness measurement," *Sensors Actuators, A Phys.* (2002).
235. L. C. Chen and Y. W. Chang, "High Accuracy Confocal Full-Field 3-D Surface Profilometry for Micro Lenses Using a Digital Fringe Projection Strategy," *Key Eng. Mater.* **364–366**, 113–116 (2007).
236. J. Burke, T. Bothe, W. Osten, and C. F. Hess, "Reverse engineering by fringe projection," in *Interferometry XI: Applications*, W. Osten, ed. (2002), p. 312.
237. C. H. Lin, H. T. He, H. W. Guo, M. Y. Chen, X. Shi, and T. Yu, "Fringe projection measurement system in reverse engineering," *J. Shanghai Univ.* (2005).

238. H. N. Yen, D. M. Tsai, and J. Y. Yang, "Full-field 3-D measurement of solder pastes using LCD-based phase shifting techniques," *IEEE Trans. Electron. Packag. Manuf.* (2006).
239. T. W. Hui and G. K. H. Pang, "Solder paste inspection using region-based defect detection," *Int. J. Adv. Manuf. Technol.* (2009).
240. D. Ambrosini, "Heat transfer measurement by a diffractive optical element fringe projection," *Opt. Eng.* **46**(9), 093606 (2007).
241. S. Tan, D. Song, and L. Zeng, "A tracking fringe method for measuring the shape and position of a swimming fish," *Opt. Commun.* **173**(1–6), 123–128 (2000).
242. F. Yuan, D. Song, and L. Zeng, "Measuring 3D profile and position of a moving object in large measurement range by using tracking fringe pattern," *Opt. Commun.* (2001).
243. G. Zhou, Z. Li, C. Wang, and Y. Shi, "A novel method for human expression rapid reconstruction," *Tsinghua Sci. Technol.* (2009).
244. G. S. Spagnolo, D. Ambrosini, and D. Paoletti, "Low-Cost Optoelectronic System for Three-Dimensional Artwork Texture Measurement," *IEEE Trans. Image Process.* **13**(3), 390–396 (2004).
245. G. Sansoni and F. Docchio, "3-D optical measurements in the field of cultural heritage: The case of the Vittoria Alata of Brescia," *IEEE Trans. Instrum. Meas.* (2005).
246. S. Gai and F. Da, "Fringe image analysis based on the amplitude modulation method," *Opt. Express* (2010).
247. A. Brahm, C. Rößler, P. Dietrich, S. Heist, P. Kühmstedt, and G. Notni, "Non-destructive 3D shape measurement of transparent and black objects with thermal fringes," in *Dimensional Optical Metrology and Inspection for Practical Applications V* (2016).
248. T. Bothe, W. Li, C. von Kopylow, and W. P. O. Juptner, "High-resolution 3D shape measurement on specular surfaces by fringe reflection," in *Optical Metrology in Production Engineering* (2004).
249. I. Simonsen, "Optics of surface disordered systems," *Eur. Phys. J. Spec. Top.* (2010).
250. E. Hecht, "Optics (4th Ed., 2003)," in *Addison Wesley* (Addison Wesley, 2003).
251. V. K. Chhaniwal, C. S. Narayanamurthy, and A. Anand, "Imaging of mass transfer process using artificial fringe deflection," *Opt. Eng.* (2014).
252. N. Yu, P. Genevet, M. A. Kats, F. Aieta, J. P. Tetienne, F. Capasso, and Z. Gaburro, "Light propagation with phase discontinuities: Generalized laws of reflection and refraction," *Science* (80-. ). (2011).

253. E. Wolf and M. Born, "Principles Of Optics," in *Pergamon Press* (1970).
254. M. Takeda, H. Ina, and S. Kobayashi, "Fourier-Transform method Of Fringe-Pattern analysis for Computer-based Topography and Interferometry," *J. Opt. Soc. Am.* (1982).
255. V. Trivedi, M. Joglekar, S. Mahajan, V. Chhaniwal, B. Javidi, and A. Anand, "Portable device based on beam deflection for refractive index mapping and diffusion coefficient measurement," *Opt. Eng.* **58**(01), 1 (2019).
256. and S. K. Mitsuo Takeda, Hideki Ina, "Fourier-transform method of fringe-pattern analysis for computer-based topography and interferometry," *J. Opt. Soc. Am.* **72**(1), 156–160 (1982).
257. V. Chhaniwal, S. Mahajan, V. Trivedi, and A. Anand, "Diffusivity measurement using compact low cost field portable device based on light deflection," in *Optical Measurement Systems for Industrial Inspection IX* (2015).
258. M. Mir, K. Tangella, and G. Popescu, "Blood testing at the single cell level using quantitative phase and amplitude microscopy," *Biomed. Opt. Express* (2011).
259. G. GAMOW, "The Evolution of the Universe," *Nature* **162**(4122), 680–682 (1948).
260. P. Hariharan, *Basics of Holography* (2002).
261. Z. El-Schish, A. Mölder, M. Sebesta, L. Gisselsson, K. Alm, and G. W. A, "Digital holographic microscopy – innovative and non-destructive analysis of living cells," *Microsc. Sci. Technol. Appl. Educ.* 1055–1062 (2010).
262. N. T. Shaked, M. T. Rinehart, and A. Wax, "Dual-interference-channel quantitative-phase microscopy of live cell dynamics," *Opt. Lett.* **34**(6), 767 (2009).
263. U. Schnars and W. Jüptner, "Direct recording of holograms by a CCD target and numerical reconstruction," *Appl. Opt.* (1994).
264. U. Schnars and W. P. O. Jüptner, "Digital recording and reconstruction of holograms in hologram interferometry and shearography," *Appl. Opt.* (1994).
265. U. Schnars, "Direct phase determination in hologram interferometry with use of digitally recorded holograms," *J. Opt. Soc. Am. A* (1994).
266. A. Asundi and V. R. Singh, "Amplitude and phase analysis in digital dynamic holography," *Opt. Lett.* (2006).
267. U. Schnars and W. Juptner, "Digital recording and numerical," *Inst. Phys. Publ.* **13**, 17 (2002).
268. S. Schedin, G. Pedrini, H. J. Tiziani, and F. Mendoza Santoyo, "Simultaneous three-dimensional dynamic deformation measurements with pulsed digital holography," *Appl. Opt.* (1999).

269. B. Nilsson, "Simultaneous measurement of shape and deformation using digital light-in-flight recording by holography," *Opt. Eng.* (2000).
270. A. Anand, V. K. Chhaniwal, and C. S. Narayanamurthy, "Diffusivity studies of transparent liquid solutions by use of digital holographic interferometry," *Appl. Opt.* (2006).
271. M. K. Kim, L. Yu, and C. J. Mann, "Interference techniques in digital holography," *J. Opt. A Pure Appl. Opt.* **8**(7), S518–S523 (2006).
272. S. De Nicola, A. Finizio, G. Pierattini, P. Ferraro, and D. Alfieri, "Angular spectrum method with correction of anamorphism for numerical reconstruction of digital holograms on tilted planes," *Opt. Express* (2005).
273. K. Matsushima and T. Shimobaba, "Band-limited angular spectrum method for numerical simulation of free-space propagation in far and near fields," *Opt. Express* (2009).
274. D. G. Voelz, *Computational Fourier Optics: A MATLAB Tutorial* (2011).
275. F. Palacios, J. Ricardo, D. Palacios, E. Gonçalves, J. L. Valin, and R. De Souza, "3D image reconstruction of transparent microscopic objects using digital holography," *Opt. Commun.* (2005).
276. M. Hammer, D. Schweitzer, B. Michel, E. Thamm, and A. Kolb, "Single scattering by red blood cells," *Appl. Opt.* (1998).
277. S. Ebrahimi, M. Dashtdar, A. Anand, and B. Javidi, "Common-path lensless digital holographic microscope employing a Fresnel biprism," *Opt. Lasers Eng.* (2020).
278. C. Hayes-Rounds, B. Bogue-Jimenez, J. Garcia-Sucerquia, O. Skalli, and A. Doblaz, "Advantages of Fresnel biprism-based digital holographic microscopy in quantitative phase imaging," *J. Biomed. Opt.* (2020).
279. F. Yuan, C. J. Yuan, S. P. Nie, Z. Q. Zhu, Q. Y. Ma, Y. Li, W. Y. Zhu, and S. T. Feng, "Digital holographic microscope employing dual-Lloyd's mirror," *Wuli Xuebao/Acta Phys. Sin.* (2014).
280. E. J. Saccocio, "Application of Lloyd's Mirror to X-Ray Holography\*," *J. Opt. Soc. Am.* (1967).
281. B. Culshaw, "The optical fibre Sagnac interferometer: An overview of its principles and applications," in *Measurement Science and Technology* (2006).
282. M. W. Kudenov, M. E. L. Jungwirth, E. L. Dereniak, and G. R. Gerhart, "White-light Sagnac interferometer for snapshot multispectral imaging," *Appl. Opt.* (2010).
283. G. D. Boreman, "Limiting aspect ratios of Sagnac interferometers," *Opt. Eng.* (2003).

284. C. Ma, Y. Li, J. Zhang, P. Li, T. Xi, J. Di, and J. Zhao, "Lateral shearing common-path digital holographic microscopy based on a slightly trapezoid Sagnac interferometer," *Opt. Express* (2017).
285. J. Běhal, "Quantitative phase imaging in common-path cross-referenced holographic microscopy using double-exposure method," *Sci. Rep.* (2019).
286. G. von Bally, "Medical applications of holography," in L. O. Svaasand, ed. (1991), pp. 2–8.
287. J. W. Goodman, "An introduction to the principles and applications of holography," *Proc. IEEE* **59**(9), 1292–1304 (1971).
288. W. E. Kock, *Engineering Applications of Lasers and Holography* (Springer US, 1975).
289. R. J. Parker, "Industrial application of holographic interferometry," in *Optical Methods in Engineering Metrology* (Springer Netherlands, 1993), pp. 213–274.
290. C. Wagner, S. Seebacher, W. Osten, and W. Jüptner, "Digital recording and numerical reconstruction of lensless Fourier holograms in optical metrology," *Appl. Opt.* **38**(22), 4812 (1999).
291. E. Serabyn, K. Liewer, and K. Wallace, "Lensless digital holographic microscopy as a means to search for life in the solar system," in *2018 IEEE Aerospace Conference* (IEEE, 2018), **2018-March**, pp. 1–7.
292. M. K. Kim, "Principles and techniques of digital holographic microscopy," *J. Photonics Energy* **1**(1), 018005 (2010).
293. H. J. Kreuzer and R. A. Pawlitzek, "Digital in-line holography," *Europhys. News* **34**(2), 62–65 (2003).
294. P.-A. J. Blanche, "Off-axis Transmission Hologram (Leith and Upatnieks)," in *Field Guide to Holography* (Society of Photo-Optical Instrumentation Engineers, 2014).
295. N. Verrier and M. Atlan, "Off-axis digital hologram reconstruction: Some practical considerations," *Appl. Opt.* (2011).
296. V. R. Singh, E. Darakis, G. Hegde, and A. Asundi, "A new methodology for pixel size retention in lensless digital holographic microscopy applied to micro-particle analysis," *J. Opt.* (2011).
297. J. P. Ryle, S. McDonnell, and J. T. Sheridan, "Lensless multispectral digital in-line holographic microscope," *J. Biomed. Opt.* **16**(12), 126004 (2011).
298. J. Garcia-Sucerquia, "Multispectral digital lensless holographic microscopy: From femtosecond laser to white light LED," in *Journal of Physics: Conference Series* (2015).

299. M. Rostykus, F. Soulez, M. Unser, and C. Moser, "Compact in-line lensfree digital holographic microscope," *Methods* **136**, 17–23 (2018).
300. L. Repetto, E. Piano, and C. Pontiggia, "Lensless digital holographic microscope with light-emitting diode illumination," *Opt. Lett.* **29**(10), 1132 (2004).
301. M. Rostykus and C. Moser, "Compact lensless off-axis transmission digital holographic microscope," *Opt. Express* (2017).
302. E. Serabyn, K. Liewer, C. Lindensmith, K. Wallace, and J. Nadeau, "Compact, lensless digital holographic microscope for remote microbiology," *Opt. Express* (2016).
303. J. Garcia-Sucerquia, "Microscopia holográfica digital sin lentes y aplicaciones," *Ing. y Compet.* (2017).
304. L. Göring, M. Finkeldey, A. Adinda-Ougba, N. C. Gerhardt, and M. Hofmann, "Lensless digital holographic microscope using in-line configuration and laser diode illumination," in *Practical Holography XXXI: Materials and Applications* (2017).
305. C. Gerhard, *Lens Design Basics* (IOP Publishing Ltd, 2020).
306. F. Heide, M. Rouf, M. B. Hullin, B. Labitzke, A. Kolb, and W. Heidrich, "Computational methods for aberration correction in simple lens imaging," *SPIE Newsroom* (2014).
307. S.-W. Chung, "Removing chromatic aberration by digital image processing," *Opt. Eng.* **49**(6), 067002 (2010).
308. T. Yue, J. Suo, J. Wang, Xun Cao, and Q. Dai, "Blind optical aberration correction by exploring geometric and visual priors," in *2015 IEEE Conference on Computer Vision and Pattern Recognition (CVPR)* (IEEE, 2015), pp. 1684–1692.
309. J. Cui and W. Huang, "Optical aberration correction for simple lenses via sparse representation," *Opt. Commun.* (2018).
310. R. A. Carreras, G. L. Tarr, S. R. Restaino, G. C. Loos, and M. Damodaran, "Concurrent computation of Zernike coefficients used in a phase diversity algorithm for optical aberration correction," in *Proceedings Volume 2315, Image and Signal Processing for Remote Sensing*, J. Desachy, ed. (1994), pp. 363–370.
311. A. J. del Águila-Carrasco, S. A. Read, R. Montés-Micó, and D. R. Iskander, "The effect of aberrations on objectively assessed image quality and depth of focus," *J. Vis.* **17**(2), 2 (2017).
312. J. Upatnieks, A. Vander Lugt, and E. Leith, "Correction of Lens Aberrations by Means of Holograms," *Appl. Opt.* (1966).
313. E. Serabyn, K. Liewer, K. Wallace, S. Rider, C. Lindensmith, and J. Nadeau, "Lensless Digital Holographic Microscopy for Microbe Detection," in *Imaging and Applied*

*Optics 2016* (OSA, 2016), p. DTh3F.4.

314. J. P. Ryle, K. M. Molony, S. McDonnell, T. J. Naughton, and J. T. Sheridan, "Multispectral lensless digital holographic microscope: imaging MCF-7 and MDA-MB-231 cancer cell cultures," in *Proc. of SPIE*, K. M. Iftekharuddin and A. A. S. Awwal, eds. (2009), p. 744206.
315. Y. Wu and A. Ozcan, "Lensless digital holographic microscopy and its applications in biomedicine and environmental monitoring," *Methods* (2018).
316. E. Serabyn, K. Liewer, and J. K. Wallace, "Resolution optimization of an off-axis lensless digital holographic microscope," *Appl. Opt.* **57**(1), A172 (2018).
317. S. Seo, T. W. Su, D. K. Tseng, A. Erlinger, and A. Ozcan, "Lensfree holographic imaging for on-chip cytometry and diagnostics," *Lab Chip* (2009).
318. A. Greenbaum, W. Luo, T. W. Su, Z. Göröcs, L. Xue, S. O. Isikman, A. F. Coskun, O. Mudanyali, and A. Ozcan, "Imaging without lenses: Achievements and remaining challenges of wide-field on-chip microscopy," *Nat. Methods* (2012).
319. S. O. Isikman, W. Bishara, S. Mavandadi, F. W. Yu, S. Feng, R. Lau, and A. Ozcan, "Lens-free optical tomographic microscope with a large imaging volume on a chip," *Proc. Natl. Acad. Sci. U. S. A.* (2011).
320. I. Pushkarsky, Y. Liu, W. Weaver, T.-W. Su, O. Mudanyali, A. Ozcan, and D. Di Carlo, "Automated single-cell motility analysis on a chip using lensfree microscopy," *Sci. Rep.* **4**(1), 4717 (2014).
321. P. Langehanenberg, B. Kemper, D. Dirksen, and G. Von Bally, "Autofocusing in digital holographic phase contrast microscopy on pure phase objects for live cell imaging," *Appl. Opt.* (2008).
322. P. Russo, *Handbook of X-Ray Imaging* (CRC Press, 2017).
323. E. Samei and N. J. Pelc, *Computed Tomography: Approaches, Applications, and Operations* (2019).
324. R. Ansorge and M. Graves, *The Physics and Mathematics of MRI* (2016).
325. A. Granov, L. Tiutin, and T. Schwarz, *Positron Emission Tomography* (2013).
326. A. Elliott, "Medical imaging," *Nucl. Instruments Methods Phys. Res. A* **546**(7473), 1–13 (2005).
327. M. R. H. David Huang, Joel Schuman, "Optical coherence tomography," *Science* (80-.). **254**(4), 1178–1181 (1991).
328. H. Kasban, M. A. M. El-Bendary, and D. H. Salama, *A Comparative Study of Medical Imaging Techniques* (2015).

329. A. Arranz and J. Ripoll, "Advances in optical imaging for pharmacological studies," *Front. Pharmacol.* (2015).
330. Z. J. Wang, T.-T. A. Chang, and R. Slauter, "Use of Imaging for Preclinical Evaluation," in *A Comprehensive Guide to Toxicology in Nonclinical Drug Development* (2017).
331. G. Pirovano, S. Roberts, S. Kossatz, and T. Reiner, "Optical imaging modalities: Principles and applications in preclinical research and clinical settings," *J. Nucl. Med.* (2020).
332. J. G. Fujimoto, C. Pitris, S. A. Boppart, and M. E. Brezinski, "Optical Coherence Tomography: An Emerging Technology for Biomedical Imaging and Optical Biopsy," *Neoplasia* **2**(1–2), 9–25 (2000).
333. C. K. H. and T. L. A F Fercher, W Drexler, "Optical coherence tomography—principles and applications," *Rep.Prog.phys* **66**, 239–303 (2003).
334. W. Drexler, H. Sattmann, B. Hermann, T. H. Ko, M. Stur, A. Unterhuber, C. Scholda, O. Findl, M. Wirtitsch, J. G. Fujimoto, and A. F. Fercher, "Enhanced visualization of macular pathology with the use of ultrahigh-resolution optical coherence tomography," *Arch. Ophthalmol.* **121**(5), 695–706 (2003).
335. M. E. Brezinski and J. G. Fujimoto, "Optical coherence tomography: high-resolution imaging in nontransparent tissue," *IEEE J. Sel. Top. Quantum Electron.* **5**(4), 1185–1192 (1999).
336. J. F. Bille, *High Resolution Imaging in Microscopy and Ophthalmology* (Springer International Publishing, 2019).
337. A. J. W. A. Yasin Alibhai, Chris Or, "Swept source optical coherence tomography: a technology review," *Curr. Ophthalmol. Rep.* **6**, 7–16 (2018).
338. X. Shu, L. Beckmann, and H. F. Zhang, "Visible-light optical coherence tomography: a review," *J. Biomed. Opt.* **22**(12), 1 (2017).
339. A. M. Zysk, F. T. Nguyen, A. L. Oldenburg, D. L. Marks, and S. A. Boppart, "Optical coherence tomography: a review of clinical development from bench to bedside," *J. Biomed. Opt.* **12**(5), 051403 (2007).
340. J. M. Schmitt, "Optical Coherence Tomography (OCT): a review," *IEEE J. Sel. Top. Quantum Electron.* **5**(4), 1205–1215 (1999).
341. D. Thomas and G. Duguid, "Optical coherence tomography - A review of the principles and contemporary uses in retinal investigation," *Eye* **18**(6), 561–570 (2004).
342. O. Thouvenin, K. Grieve, P. Xiao, C. Apelian, and A. C. Boccara, "En face coherence microscopy [Invited]," *Biomed. Opt. Express* **8**(2), 622 (2017).

343. T. Schmoll, C. Kolbitsch, and R. A. Leitgeb, "In vivo functional retinal optical coherence tomography," *J. Biomed. Opt.* **15**(4), 041513 (2010).
344. W. Drexler, R. Leitgeb, and C. K. Hitzenberger, "New Developments in Optical Coherence Tomography Technology," in (2010), pp. 201–216.
345. H. Jelínková, *Lasers for Medical Applications* (Woodhead Publishing Limited, 2013).
346. P. Sharma, J. Kumawat, S. Kumar, K. Sahu, Y. Verma, P. K. Gupta, and K. D. Rao, "Feasibility of speckle variance OCT for imaging cutaneous microvasculature regeneration during healing of wounds in diabetic mice," *Laser Phys.* **28**(2), (2018).
347. W. Rudolph and M. Kempe, "Trends in optical biomedical imaging," *J. Mod. Opt.* **44**(9), 1617–1642 (1997).
348. A. Al-Mujaini, U. K. Wali, and S. Azeem, "Optical coherence tomography: Clinical applications in medical practice," *Oman Med. J.* **28**(2), 86–91 (2013).
349. M. Ibne Mokbul, "Optical Coherence Tomography: Basic Concepts and Applications in Neuroscience Research," *J. Med. Eng.* **2017**, 1–20 (2017).
350. Z. Yaqoob, J. Wu, and C. Yang, "Spectral domain optical coherence tomography: a better OCT imaging strategy," *Biotechniques* **39**(6S), S6–S13 (2005).
351. B. Li, H. Wang, B. Fu, R. Wang, S. Sakadžic, and D. A. Boas, "Impact of temporal resolution on estimating capillary RBC-flux with optical coherence tomography," *J. Biomed. Opt.* **22**(1), 016014 (2017).
352. U. Baran and R. K. Wang, "Review of optical coherence tomography based angiography in neuroscience," *Neurophotonics* **3**(1), 010902 (2016).
353. C. Magnain, J. C. Augustinack, M. Reuter, C. Wachinger, M. P. Frosch, T. Ragan, T. Akkin, V. J. Wedeen, D. A. Boas, and B. Fischl, "Blockface histology with optical coherence tomography: A comparison with Nissl staining," *Neuroimage* **84**, 524–533 (2014).
354. Brett E Bouma and Guillermo Tearney, *Handbook of Optical Coherence Tomography* (New York: Marcel Dekker, Inc., 2001).
355. W. Drexler and J. Fujimoto, "State-of-the-art retinal optical coherence tomography," *Prog. Retin. Eye Res.* **27**(1), 45–88 (2008).
356. M. R. Hee, "Optical Coherence Tomography of the Human Retina," *Arch. Ophthalmol.* **113**(3), 325 (1995).
357. R. F. Spaide, J. M. Klancnik, and M. J. Cooney, "Retinal Vascular Layers Imaged by Fluorescein Angiography and Optical Coherence Tomography Angiography," *JAMA Ophthalmol.* **133**(1), 45 (2015).

358. C. A. Puliafito, M. R. Hee, C. P. Lin, E. Reichel, J. S. Schuman, J. S. Duker, J. A. Izatt, E. A. Swanson, and J. G. Fujimoto, "Imaging of Macular Diseases with Optical Coherence Tomography," *Ophthalmology* **102**(2), 217–229 (1995).
359. M. Wojtkowski, R. Leitgeb, A. Kowalczyk, T. Bajraszewski, and A. F. Fercher, "In vivo human retinal imaging by Fourier domain optical coherence tomography," *J. Biomed. Opt.* **7**(3), 457 (2002).
360. T. Yonetsu, B. E. Bouma, K. Kato, J. G. Fujimoto, and I.-K. Jang, "Optical Coherence Tomography," *Circ. J.* **77**(8), 1933–1940 (2013).
361. T. Yonetsu, T. Kakuta, T. Lee, K. Takayama, K. Kakita, T. Iwamoto, N. Kawaguchi, K. Takahashi, G. Yamamoto, Y. Iesaka, H. Fujiwara, and M. Isobe, "Assessment of acute injuries and chronic intimal thickening of the radial artery after transradial coronary intervention by optical coherence tomography," *Eur. Heart J.* **31**(13), 1608–1615 (2010).
362. L. J. Diaz-Sandoval, B. E. Bouma, G. J. Tearney, and I. K. Jang, "Optical coherence tomography as a tool for percutaneous coronary interventions," *Catheter. Cardiovasc. Interv.* **65**(4), 492–496 (2005).
363. G. Souteyrand, N. Amabile, L. Mangin, X. Chabin, N. Meneveau, G. Cayla, G. Vanzetto, P. Barnay, C. Trouillet, G. Rioufol, G. Rangé, E. Teiger, R. Delaunay, O. Dubreuil, T. Lhermusier, A. Mulliez, S. Levesque, L. Belle, C. Caussin, and P. Motreff, "Mechanisms of stent thrombosis analysed by optical coherence tomography: Insights from the national PESTO French registry," *Eur. Heart J.* **37**(15), 1208-1216a (2016).
364. M. E. Brezinski, G. J. Tearney, N. J. Weissman, S. A. Boppart, B. E. Bouma, M. R. Hee, A. E. Weyman, E. A. Swanson, J. F. Southern, and J. G. Fujimoto, "Assessing atherosclerotic plaque morphology: comparison of optical coherence tomography and high frequency intravascular ultrasound.," *Heart* **77**(5), 397–403 (1997).
365. I.-K. Jang, B. E. Bouma, D.-H. Kang, S.-J. Park, S.-W. Park, K.-B. Seung, K.-B. Choi, M. Shishkov, K. Schlendorf, E. Pomerantsev, S. L. Houser, H. T. Aretz, and G. J. Tearney, "Visualization of coronary atherosclerotic plaques in patients using optical coherence tomography: comparison with intravascular ultrasound," *J. Am. Coll. Cardiol.* **39**(4), 604–609 (2002).
366. B. E. Bouma, G. J. Tearney, C. C. Compton, and N. S. Nishioka, "High-resolution imaging of the human esophagus and stomach in vivo using optical coherence tomography," *Gastrointest. Endosc.* **51**(4), 467–474 (2000).
367. A. Das, M. V. Sivak, A. Chak, R. C. K. Wong, V. Westphal, A. M. Rollins, J. Willis, G. Isenberg, and J. A. Izatt, "High-resolution endoscopic imaging of the GI tract: A comparative study of optical coherence tomography versus high-frequency catheter probe EUS," *Gastrointest. Endosc.* **54**(2), 219–224 (2001).
368. J. A. Izatt, M. D. Kulkarni, Hsing-Wen Wang, K. Kobayashi, and M. V. Sivak, "Optical coherence tomography and microscopy in gastrointestinal tissues," *IEEE J. Sel. Top. Quantum Electron.* **2**(4), 1017–1028 (1996).

369. X. D. Li, S. A. Boppart, J. Van Dam, H. Mashimo, M. Mutinga, W. Drexler, M. Klein, C. Pitris, M. L. Krinsky, M. E. Brezinski, and J. G. Fujimoto, "Optical Coherence Tomography: Advanced Technology for the Endoscopic Imaging of Barrett's Esophagus," *Endoscopy* **32**(12), 921–930 (2000).
370. G. J. Tearney, M. E. Brezinski, J. F. Southern, B. E. Bouma, S. A. Boppart, and J. G. Fujimoto, "Optical biopsy in human gastrointestinal tissue using optical coherence tomography," *Am. J. Gastroenterol.* **92**(10), 1800–4 (1997).
371. E. V. Zagaynova, N. D. Gladkova, O. S. Streltsova, G. V. Gelikonov, N. Tresser, F. I. Feldchtein, M. J. Manyak, and N. M. Shakhova, "Optical Coherence Tomography in Urology," in (Springer, Berlin, Heidelberg, 2008), pp. 1241–1268.
372. H. W. Wang and Y. Chen, "Clinical applications of optical coherence tomography in urology," *IntraVital* **3**(1), e28770-1-e28770-11 (2014).
373. J. E. Freund, M. Buijs, C. D. Savci-Heijink, D. M. de Bruin, J. J. M. C. H. de la Rosette, T. G. van Leeuwen, and M. P. Laguna, "Optical Coherence Tomography in Urologic Oncology: a Comprehensive Review," *SN Compr. Clin. Med.* **1**(2), 67–84 (2019).
374. E. V. Zagaynova, N. D. Gladkova, O. S. Streltsova, G. V. Gelikonov, N. Tresser, F. I. Feldchtein, M. J. Manyak, and N. M. Shakhova, "Optical Coherence Tomography in Urology," in (2008), pp. 1241–1268.
375. G. J. Tearney, M. E. Brezinski, J. F. Southern, B. E. Bouma, S. A. Boppart, and J. G. Fujimoto, "Optical Biopsy in Human Urologic Tissue Using Optical Coherence Tomography," *J. Urol.* **157**(5), 1915–1919 (1997).
376. E. Sattler, R. Kästle, and J. Welzel, "Optical Coherence Tomography in Dermatology," *J. Biomed. Opt.* **18**, 061224–6 (2013).
377. J. Welzel, "Optical coherence tomography in dermatology: A review," *Ski. Res. Technol.* **7**(1), 1–9 (2001).
378. J. Olsen, J. Holmes, and G. B. E. Jemec, "Advances in optical coherence tomography in dermatology—a review," *J. Biomed. Opt.* **23**(04), 040901–10 (2018).
379. T. Gambichler, V. Jaedicke, and S. Terras, "Optical coherence tomography in dermatology: Technical and clinical aspects," *Arch. Dermatol. Res.* **303**(7), 457–473 (2011).
380. M. Machoy, J. Seeliger, L. Szyszka-Sommerfeld, R. Koprowski, T. Gedrange, and K. Woźniak, "The Use of Optical Coherence Tomography in Dental Diagnostics: A State-of-the-Art Review," *J. Healthc. Eng.* **2017**, 1–31 (2017).
381. Y.-S. Hsieh, Y.-C. Ho, S.-Y. Lee, C.-C. Chuang, J. Tsai, K.-F. Lin, and C.-W. Sun, "Dental Optical Coherence Tomography," *Sensors* **13**(7), 8928–8949 (2013).
382. D. Claus, J. Radeke, M. Zint, A. B. Vogel, Y. Satravaha, F. Kilic, R. Hibst, and B. G. Lapatki, "Generation of 3D digital models of the dental arches using optical scanning

- techniques," *Semin. Orthod.* **24**(4), 416–429 (2018).
383. J. Wang, Y. Xu, and S. A. Boppart, "Review of optical coherence tomography in oncology," *J. Biomed. Opt.* **22**(12), 1 (2017).
  384. P. Si, A. Honkala, A. de la Zerda, and B. R. Smith, "Optical Microscopy and Coherence Tomography of Cancer in Living Subjects," *Trends in Cancer* **6**(3), 205–222 (2020).
  385. S. Tatebe, Y. Fukumoto, K. Sugimura, Y. Miura, K. Nochioka, T. Aoki, M. Miura, S. Yamamoto, N. Yaoita, K. Satoh, and H. Shimokawa, "Optical Coherence Tomography Is Superior to Intravascular Ultrasound for Diagnosis of Distal-Type Chronic Thromboembolic Pulmonary Hypertension," *Circ. J.* **77**(4), 1081–1083 (2013).
  386. S. K. Dubey, T. Anna, C. Shakher, and D. S. Mehta, "Fingerprint detection using full-field swept-source optical coherence tomography," *Appl. Phys. Lett.* **91**(18), 181106 (2007).
  387. S. K. Dubey, D. S. Mehta, A. Anand, and C. Shakher, "Simultaneous topography and tomography of latent fingerprints using full-field swept-source optical coherence tomography," *J. Opt. A Pure Appl. Opt.* **10**(1), 015307 (2008).
  388. S. A. Boppart, S. A. Boppart, M. E. Brezinski, C. Pitris, C. Pitris, and J. G. Fujimoto, "Optical Coherence Tomography for Neurosurgical Imaging of Human Intracortical Melanoma," *Neurosurgery* **43**(4), 834–841 (1998).
  389. S. A. Boppart, B. E. Bouma, M. E. Brezinski, G. J. Tearney, and J. G. Fujimoto, "Imaging developing neural morphology using optical coherence tomography," *J. Neurosci. Methods* **70**(1), 65–72 (1996).
  390. A. M. Rollins, M. D. Kulkarni, S. Yazdanfar, R. Ung-arunyawee, and J. A. Izatt, "In vivo video rate optical coherence tomography," *Opt. Express* **3**(6), 219 (1998).
  391. G. Popescu, Y. Park, N. Lue, C. Best-Popescu, L. Deflores, R. R. Dasari, M. S. Feld, and K. Badizadegan, "Optical imaging of cell mass and growth dynamics," *Am. J. Physiol. Physiol.* **295**(2), C538–C544 (2008).
  392. S. A. Boppart, B. E. Bouma, C. Pitris, J. F. Southern, M. E. Brezinski, and J. G. Fujimoto, "In vivo cellular optical coherence tomography imaging," *Nat. Med.* **4**(7), 861–865 (1998).
  393. M. D. Duncan, M. Bashkansky, and J. Reintjes, "Subsurface defect detection in materials using optical coherence tomography," *Opt. Express* **2**(13), 540 (1998).
  394. F. Xu, H. E. Pudavar, P. N. Prasad, and D. Dickensheets, "Confocal enhanced optical coherence tomography for nondestructive evaluation of paints and coatings," *Opt. Lett.* (1999).
  395. S. R. Chinn and E. A. Swanson, "Multilayer optical storage by low-coherence reflectometry," *Opt. Lett.* **21**(12), 899 (1996).

396. K. Takada, I. Yokohama, K. Chida, and J. Noda, "New measurement system for fault location in optical waveguide devices based on an interferometric technique," *Appl. Opt.* **26**(9), 1603 (1987).
397. A. M. Kowalewicz, T. R. Schibli, F. X. Kärtner, and J. G. Fujimoto, "Ultralow-threshold Kerr-lens mode-locked Ti:Al<sub>2</sub>O<sub>3</sub> laser," *Opt. Lett.* **27**(22), 2037 (2002).
398. D. S. Adler, T. H. Ko, A. K. Konorev, D. S. Mamedov, V. V Prokhorov, J. J. Fujimoto, and S. D. Yakubovich, "Broadband light source based on quantum-well superluminescent diodes for high-resolution optical coherence tomography," *Quantum Electron.* **34**(10), 915–918 (2004).
399. T. H. Ko, D. C. Adler, J. G. Fujimoto, D. Mamedov, V. Prokhorov, V. Shidlovski, and S. Yakubovich, "Ultrahigh resolution optical coherence tomography imaging with a broadband superluminescent diode light source," *Opt. Express* **12**(10), 2112 (2004).
400. J. P. Goure, *Optics in Instruments* (John Wiley & Sons, Inc., 2011).
401. T. L. Szabo, *Diagnostic Ultrasound Imaging: Inside Out: Second Edition* (2004).
402. D. Huang, E. A. Swanson, C. P. Lin, J. S. Schuman, W. G. Stinson, W. Chang, M. R. Hee, T. Flotte, K. Gregory, C. A. Puliafito, and J. G. Fujimoto, "Optical coherence tomography," *Science* (80-. ). (1991).
403. J. A. Izatt, M. A. Choma, and A. H. Dhalla, *Theory of Optical Coherence Tomography* (Springer, Berlin, Heidelberg, 2015).